

Stress-induced reversible cell-cycle arrest requires PRC2/PRCI-mediated control of mitophagy in *Drosophila* germline stem cells and human iPSCs

Tommy H. Taslim,^{1,2,5} Abdiasis M. Hussein,^{1,2,5} Riya Keshri,^{1,2,5} Julien R. Ishibashi,^{1,2,5} Tung C. Chan,^{1,2} Bich N. Nguyen,^{1,2} Shuozhi Liu,^{1,2} Daniel Brewer,^{1,2} Stuart Harper,^{1,2} Scott Lyons,^{1,2} Ben Garver,^{1,2} Jimmy Dang,^{1,2} Nanditaa Balachandar,^{1,2,3} Samridhi Jhajharia,^{1,2,3} Debra del Castillo,^{1,2} Julie Mathieu,^{1,2,4} and Hannele Ruohola-Baker^{1,2,*}

¹Department of Biochemistry, University of Washington, Seattle, WA, USA

²Institute for Stem Cell and Regenerative Medicine, University of Washington, School of Medicine, Seattle, WA, USA

³Department of Biotechnology, School of Bioengineering, Faculty of Engineering and Technology, SRM Institute of Science and Technology, Kattankulathur, India

⁴Department of Comparative Medicine, University of Washington, Seattle, WA, USA

⁵These authors contributed equally

*Correspondence: hannele@uw.edu

<https://doi.org/10.1016/j.stemcr.2022.11.004>

SUMMARY

Following acute genotoxic stress, both normal and tumorous stem cells can undergo cell-cycle arrest to avoid apoptosis and later re-enter the cell cycle to regenerate daughter cells. However, the mechanism of protective, reversible proliferative arrest, “quiescence,” remains unresolved. Here, we show that mitophagy is a prerequisite for reversible quiescence in both irradiated *Drosophila* germline stem cells (GSCs) and human induced pluripotent stem cells (hiPSCs). In GSCs, mitofission (Drp1) or mitophagy (Pink1/Parkin) genes are essential to enter quiescence, whereas mitochondrial biogenesis (PGC1 α) or fusion (Mfn2) genes are crucial for exiting quiescence. Furthermore, mitophagy-dependent quiescence lies downstream of mTOR- and PRC2-mediated repression and relies on the mitochondrial pool of cyclin E. Mitophagy-dependent reduction of cyclin E in GSCs and in hiPSCs during mTOR inhibition prevents the usual G1/S transition, pushing the cells toward reversible quiescence (G0). This alternative method of G1/S control may present new opportunities for therapeutic purposes.

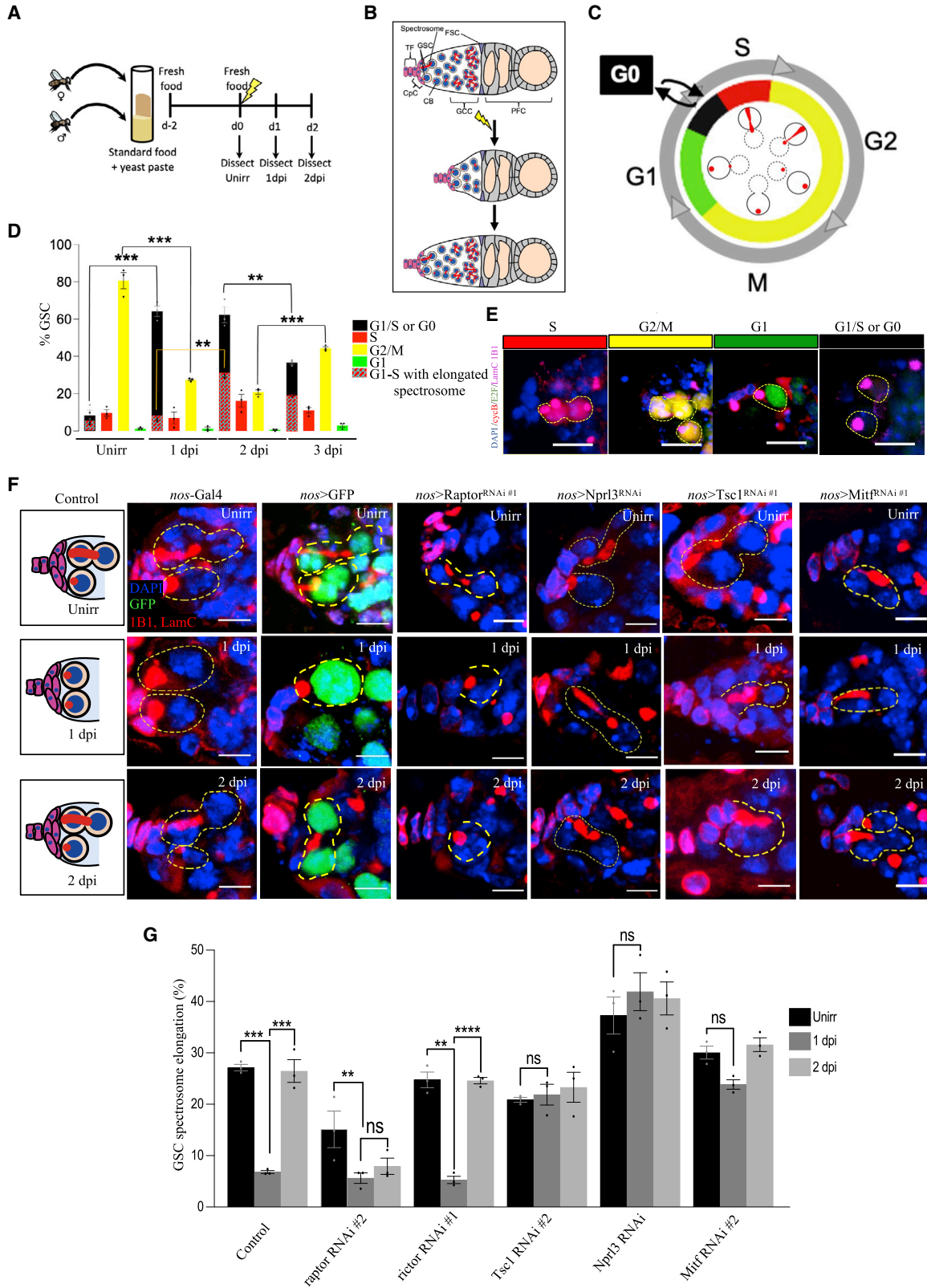
INTRODUCTION

Diverse types of stem cells have the capacity to exit the cell cycle upon stress, only to re-enter under the appropriate conditions; this process, coined “quiescence,” is distinct from senescence because quiescence can normally be reversed. Nutrient-sensitive mechanistic target of rapamycin (mTOR) signaling has been implicated in quiescence, with mTOR activation promoting proliferation and exit from quiescence, and mTOR repression being a hallmark of stem cells in quiescence (van Velthoven and Rando, 2019; Cho et al., 2019; Meng et al., 2018; Artoni et al., 2017) and embryonic diapause (Bulut-Karslioglu et al., 2016; Hussein et al., 2020; Arena et al., 2021), an extreme example of developmental quiescence, with some exceptions (Mathieu et al., 2019). Moreover, quiescence is associated with decreased mitochondrial metabolism and increased macroautophagy (van Velthoven and Rando, 2019; Cho et al., 2019), herein referred to as autophagy. Epigenetic remodeling is another hallmark of quiescent stem cell states (van Velthoven and Rando, 2019; Cho et al., 2019; Hussein et al., 2020; Somasundaram et al., 2020; Hu et al., 2020). However, it remains unknown whether there are overarching rules that control entering and exiting quiescence across different types of stem cells. It will be particularly important to identify the molecules

that distinguish reversible quiescence from DNA damage-induced apoptosis (Artoni et al., 2017; Xing et al., 2015).

DNA damage checkpoint recognizes irreparable DNA damage, inducing p53-dependent apoptosis (Aubrey et al., 2018; Speidel, 2010; Chakravarti et al., 2022; He et al., 2019). However, despite p53 activity (Hussein et al., 2020; Ma et al., 2016), stem cells in quiescence, including embryonic stem cells (ESCs) in diapause, resist apoptosis (Artoni et al., 2017; Hussein et al., 2020, 2022; Arena et al., 2021; Xing et al., 2015; Ma et al., 2016). Although it is not understood mechanistically how stem cells in general avoid apoptosis, in the germline stem cells (GSCs) of the adult *Drosophila* ovary at least one protective mechanism has been identified. GSCs in the somatic niche undergo self-renewing divisions to produce a cystoblast (CB) and a new GSC. The cystoblast further undergoes four incomplete cell divisions and eventually produces one oocyte connected to support cells called nurse cells; therefore, the GSCs are maintained in the somatic niche of the germaria to regenerate the oocyte pool. GSCs can survive genotoxic stress such as ionizing radiation (IR) by entering a reversible state of quiescence. In contrast, the GSC differentiating progenies undergo apoptosis and support survival of the GSCs (Xing et al., 2015). This reversible, protective GSC halt of the cell cycle allows regeneration of the germ line after insult (Artoni et al., 2017; Xing et al.,





(legend on next page)



2015; Ma et al., 2016; Ishibashi et al., 2020, 2021) (Figures 1A and 1B). The stress-response transcription factor FOXO and the metabolic kinase mTOR were shown to be crucial for the entry into and exit from quiescence, respectively (Artoni et al., 2017). However, it is not yet known which mTOR targets are critical for the regulation of quiescence or how cell-cycle re-entry from GSC quiescence is so precisely timed.

In this study, we show that mTOR activity regulates the key epigenetic modifiers, PRC1/2, necessary for insult-induced mitophagy that results in quiescence. We further show that the mechanism of insult-induced quiescence relies on mitochondrial dynamics to temporally regulate a mitochondrial pool of cyclin E (CycE). Not only *Drosophila* GSCs, but also human induced pluripotent stem cells (hiPSCs) couple cell-cycle progression to mitochondrial quantity via the mitochondrial reserve of CycE.

RESULTS

mTORC1 inhibition is necessary for IR-induced entry into quiescence in *Drosophila* GSCs

To dissect the GSC reversible cell-cycle block in more detail we employed the IR-induced insult paradigm and fly fluorescent ubiquitination-based cell-cycle indicator (FUCCI) to visualize distinct cell-cycle stages in GSCs (Zielke et al., 2014) (Figures 1C–1E). In the fly FUCCI line GFP-E2F1_{1–230} is degraded by ubiquitin ligase CRL4^{Cdt2} in S phase, and mRFP-CycB_{1–266} is degraded by APC/C in late mitosis/G1 (Figures 1C and 1E) (Zielke et al., 2014; Villa-Fombuena et al., 2021). Hence, FUCCI cells are green (GFP⁺/RFP⁻) in G1, red (GFP⁻/RFP⁺) in S, yellow (GFP⁺/RFP⁺) in G2/M, and black (GFP⁻/RFP⁻) in the G1-S transition (Figures 1C–1E). In the unirradiated control we observed a distribution of GSCs in (80%) G2/M, (8%) S, (1%) G1, and (8%) G1-S transition (Figures 1C and 1D),

similar to previous findings (Villa-Fombuena et al., 2021). In contrast, 1 day post-insult (1 dpi) shows a significant increase in black GSCs (60%) (Figure 1D), a state of G0 quiescence. Further, 3 dpi shows a significant reduction in G0 with significant increase in G2/M (Figure 1D). At 2 dpi, when GSCs expectedly exit quiescence, we observe no significant reduction in black GSCs (Figure 1D). Upon analysis of the division marker phosphorylated serine 10 residue on histone 3 (PH3⁺) in GSCs, we found that 2.3%, 0.3%, and 1.9% of GSCs are PH3⁺ when unirradiated and at 1 and 2 dpi, respectively (Figure S1C), suggesting reversion of quiescence by 2 dpi (Figures S1B and S1C). To reconcile, we further analyzed another cell-cycle marker, GSC spectroosome elongation (Villa-Fombuena et al., 2021). The unirradiated GSCs showed an elongated spectroosome in S phase (or early G2) (Villa-Fombuena et al., 2021) (Figures 1C and 1F). At 1 dpi GSCs showed a significant reduction in elongated spectroosomes, whereas at 2 dpi the normal percentage of elongated spectroosomes was observed again, indicating the exit from quiescence (Figure 1F). Therefore, we proceeded to use elongated spectroosomes as a proxy for GSC division (Figures 1C, 1F, and 1G) (Artoni et al., 2017; Xing et al., 2015). We further categorized black GSCs in the FUCCI line into (1) unelongated, (2) elongated, or (3) partially elongated spectroosome type. When unirradiated, the rare black GSCs mainly showed partially elongated spectroosomes. At 1 dpi, black GSCs commonly have unelongated spectroosomes (75%) and partially elongated (25%) spectroosomes. Strikingly, at 2 dpi, we observed a significant increase in elongated spectroosomes, to 50% of black GSCs (Figures 1D and 1E), indicating G1-S transition (Figure 1C; Villa-Fombuena et al., 2021); hence, the GSCs appear to have mostly exited G0 or quiescence.

We sought to dissect the molecular role of the mTOR and its components to regulate quiescence. In wild-type (WT) control flies (*nos*-Gal4 driver), 27% of GSCs are in S phase

Figure 1. Role of mTORC1 in regulating insult-induced quiescence in female GSCs

(A) Experimental setup for irradiation model.

(B) Representative diagram of a germarium in the *Drosophila* ovary before and after IR. TF, terminal filament cell; CpC, cap cell; GSC, germline stem cell; CB, undifferentiated cystoblast; FSC, follicle stem cell; PFC, prefollicle cell.

(C) Schematic of various cell-cycled stages of GSCs, correlated with the expression pattern of GFP-E2F1_{1–230} and mRFP-CycB_{1–266} in GSCs. (D) Percentage of cells positive for mRFP-CycB_{1–266} (red) or GFP-E2F1_{1–230} (green), dual positive mRFP-CycB_{1–266} GFP-E2F1_{1–230} (yellow), or expressing none of the fluorophore (black) under unirradiated, 1-day post-insult (1 dpi), 2 dpi, and 3 dpi conditions. Black represents G1/S or G0 phase, red represents S phase, yellow represents G2/M stage, and green represents G1 stage, while within the black bar the red dotted bar represents a percentage of cells in G1/S phase only, as these are the cells with elongated spectroosome.

(E) Representative images of GSCs in the fly FUCCI line expressing GFP-E2F1_{1–230} and mRFP-CycB_{1–266}. Dotted circle represents GSC (scale bar, 5 μm).

(F) Representative confocal microscopy images of control (*nos*-Gal4 and *nos*>GFP) and listed UAS-RNAi KD from unirradiated, 1 dpi, and 2 dpi germaria stained with 1B1 (red, spectroosomes/fusomes), LamC (red, CpC and TF), and DAPI (blue, nuclei), as well as GFP (green, GSCs and progeny). Dotted circle represents GSC (scale bar, 5 μm).

(G) Percentage of GSCs showing spectroosome elongation. *p ≤ 0.05, **p ≤ 0.01, and ***p ≤ 0.001.



with elongated spectrosomes (ESs; [Figures 1F and 1G](#)). At 1 dpi, the GSCs enter a state of quiescence (5% ES), and at 2 dpi GSCs successfully exit quiescence and resume cell division (27% ES; [Figures 1F and 1G](#)). Knockdown (KD) of the mTORC1 component raptor by RNAi moderately decreases rates of GSC division (12% ES) ([Figures 1F and 1G](#)), consistent with mTORC1 activity promoting cell division ([Artoni et al., 2017](#)). At 1 dpi the raptor KD GSCs efficiently enter IR-induced quiescence (2% ES), but strikingly, GSC division remains low at 2 dpi (3% ES), indicating a failure to exit quiescence ([Figures 1F and 1G](#)). In contrast, KD of the mTORC2 component rictor by RNAi has no appreciable effect on unirradiated rates of division (25% ES), and the GSCs properly arrest division at 1 dpi (5% ES) and resume division at 2 dpi (25% ES) ([Figures 1G and S1A and Table S1](#)), similar to WT controls, suggesting that mTORC2 might be functionally dispensable in GSC insult-induced quiescence. Altogether, these data show that mTORC1 activation is necessary for the exit from quiescence.

mTOR regulatory complexes TSC and GATOR1 are known to inhibit mTOR activity, while GATOR2 inhibits GATOR1 and can thereby activate mTORC1 ([Kim and Guan, 2019; Wei et al., 2019](#)). When the TSC component Tsc1 was knocked down by RNAi in GSCs, the rate of GSC division remained unchanged (unirradiated, 22% ES; 1 dpi, 21% ES; 2 dpi, 24% ES) ([Figures 1F and 1G](#)), suggesting that Tsc1 is required for quiescence. Similarly, when the GATOR1 component Nprl3 is knocked down, the GSCs do not block the cell cycle after insult (unirradiated, 37.5% ES; 1 dpi, 44.5% ES; 2 dpi, 43.5% ES) ([Figures 1F and 1G](#)). KD of another GATOR1 component, Nprl2, showed a similar inability to arrest cell division ([Table S1](#)), suggesting that GATOR1-mediated mTORC1 inhibition is essential for insult-induced quiescence. Intriguingly, GSCs with GATOR2 component (Nup44a and Mio) KD are comparable to WT controls ([Table S1](#)). These data are consistent with earlier findings that both TSC and GATOR1 become activated in response to the programmed DNA double-strand break during meiosis to mitigate genotoxic stress ([Wei et al., 2019](#)), and that GATOR2 is not appreciably active in GSCs ([Wei et al., 2014](#)). In conclusion, mTORC1 repression is essential to enter insult-induced quiescence in GSC.

During stress, mTORC1 inactivation results in transcription factor MITF/TFEB/TFE3 dephosphorylation, resulting in its nuclear translocation ([Settembre et al., 2011](#)). In *Drosophila* Mitf is the single identified MITF-TFE family member. Mitf can regulate V-ATPase expression that results in amino-acid-dependent activation of mTOR. mTORC1 then can phosphorylate and sequester *Drosophila* Mitf in the cytoplasm, leading to Mitf transcriptional inactivation through this feedback loop ([Zhang et al., 2015](#)). In addition, mammalian Mitf is shown to act in a multitude of

other biological processes ([Goding and Arnheiter, 2019](#)). We sought to test the role of Mitf in *Drosophila* GSC IR-induced quiescence. Mitf KD abrogates insult-induced quiescence, as division rates at 1 dpi remain high ([Figures 1F and 1G](#)), suggesting that mTORC1 regulates GSC quiescence via Mitf-transcriptional targets, such as autophagy genes ([Bouché et al., 2016](#)).

Autophagy-deficient GSCs fail to enter into quiescence

We analyzed if mTORC1/Mitf-dependent autophagy regulates GSC quiescence. To characterize autophagy upon irradiation, we used the *nos>mCherry-Atg8a* (a reporter of autophagosome/autolysosome formation) line ([Mauvezin et al., 2014](#)). We observed a basal level of autophagy before irradiation, where 35% of GSCs contain mCherry-Atg8a puncta ([Figures 2A and S2A–S2C](#)). The number of GSCs with puncta increased at 1 dpi (87%) and reduced at 2 dpi (54%) ([Figures 2A and S2A–S2C](#)), indicating that autophagosomes/autolysosomes are acutely upregulated at GSC quiescence. To further characterize the rate of autophagic flux, we analyzed *nos>GFP-mCherry-Atg8a* GSCs. Unlike mCherry fluorescence, GFP is highly sensitive to pH, and therefore quenches in the low pH of the autolysosome ([Mauvezin et al., 2014](#)). Using this reporter, autophagosomes are expected to be yellow (GFP⁺/mCherry⁺), while autolysosomes are expected to be red (GFP⁻/mCherry⁺) ([Figure S2A](#)). Interestingly, we observed only red puncta, suggesting that, in GSCs, mature autophagosomes are rapidly acidified, characteristic of high autophagic flux ([Figures 2A, 2B, and S2C](#)). These data align with past results in hematopoietic stem cells suggesting that quiescence is characterized, in part, by the accumulation of autolysosomes ([Liang et al., 2020](#)).

Autophagy activation by either overexpression of Atg1, an inducer of autophagy, ([Figures S2D and S2E](#)), or KD of Rubicon, an inhibitor of autophagy ([Table S1](#)), prevented complete cell-cycle re-entry at 2 dpi, suggesting that dampening of autophagy is required to exit from quiescence. Atg1 has previously been reported to be phosphorylated by CDK1/cyclin B and is necessary for cell-cycle progression, which potentially explains the high basal division rate at 1 and 2 dpi in Atg1-overexpressing GSCs. Conversely, depletion of the core autophagy genes involved in phagophore nucleation, autophagic membrane elongation, or autophagosome maturation impaired the entrance into quiescence (Atg14, 18a, 3, 7, 12, 16; [Figures 2C, 2D, and S2D and Table S1](#)). These data align with findings that mouse ESCs arrest cell division upon chemical induction of autophagy ([Suvorova et al., 2019](#)), suggesting autophagy may be a more universal regulator of stem cell state.

Mitophagy acts downstream of IR-induced autophagy

Mitochondrial autophagy (mitophagy) and mitochondrial remodeling are important cellular processes that, when

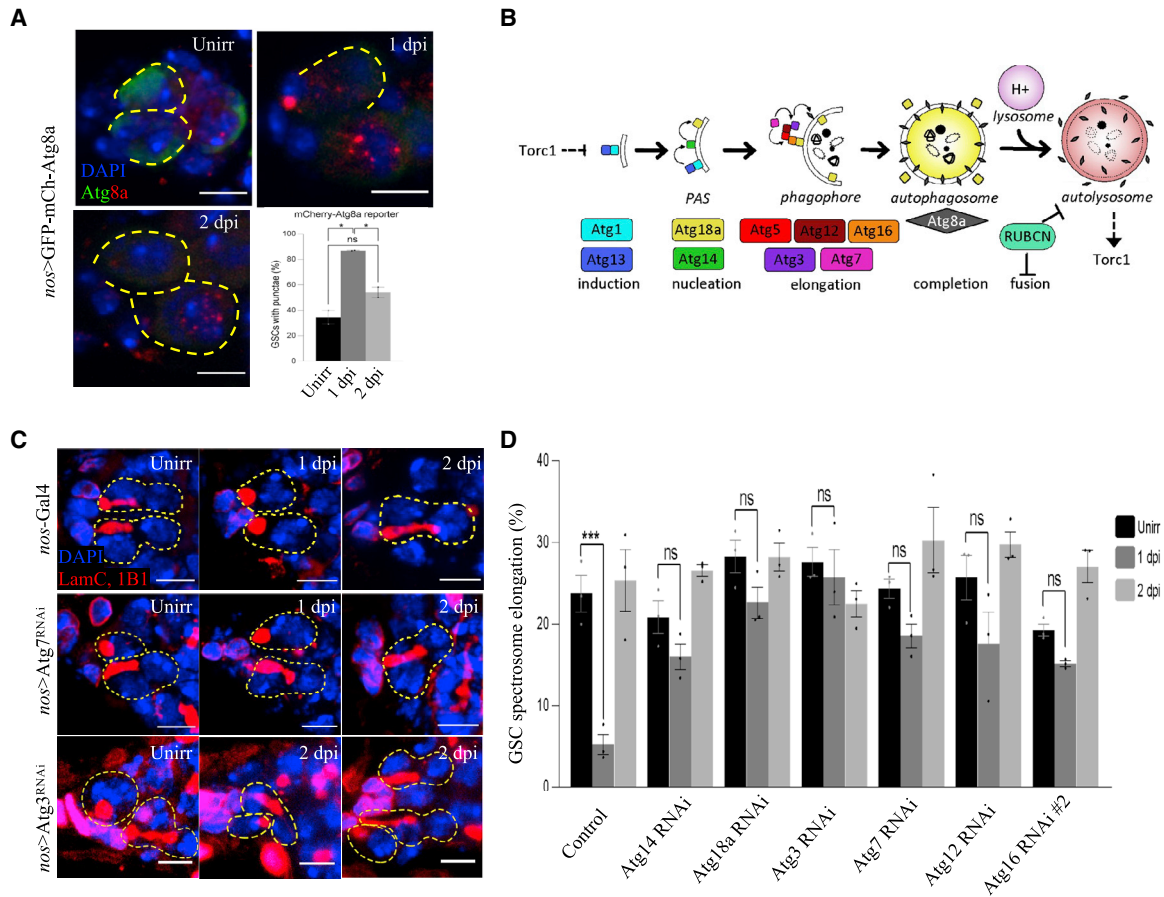


Figure 2. Autophagy-defective germline stem cells display impaired quiescence

(A) Representative confocal microscopy images of *nos>GFP-mCherry-Atg8a* from unirradiated, 1 dpi, and 2 dpi germaria stained with GFP (green, cytoplasm/autophagosome), mCherry (red, autophagosome/autolysosome), and DAPI (blue, nuclei). Dotted circle represents GSC (scale bars, 5 μ m). The graph shows quantification of puncta in *nos>mCherry-Atg8a* germaria, stained with mCherry. A portion of unirradiated GSCs (35%) contain >1 mCherry puncta. At 1 dpi, this increases sharply (87%), suggesting an acute increase in autophagic degradation. By 2 dpi, GSCs with puncta decrease (54%), concurrent with the exit from quiescence.

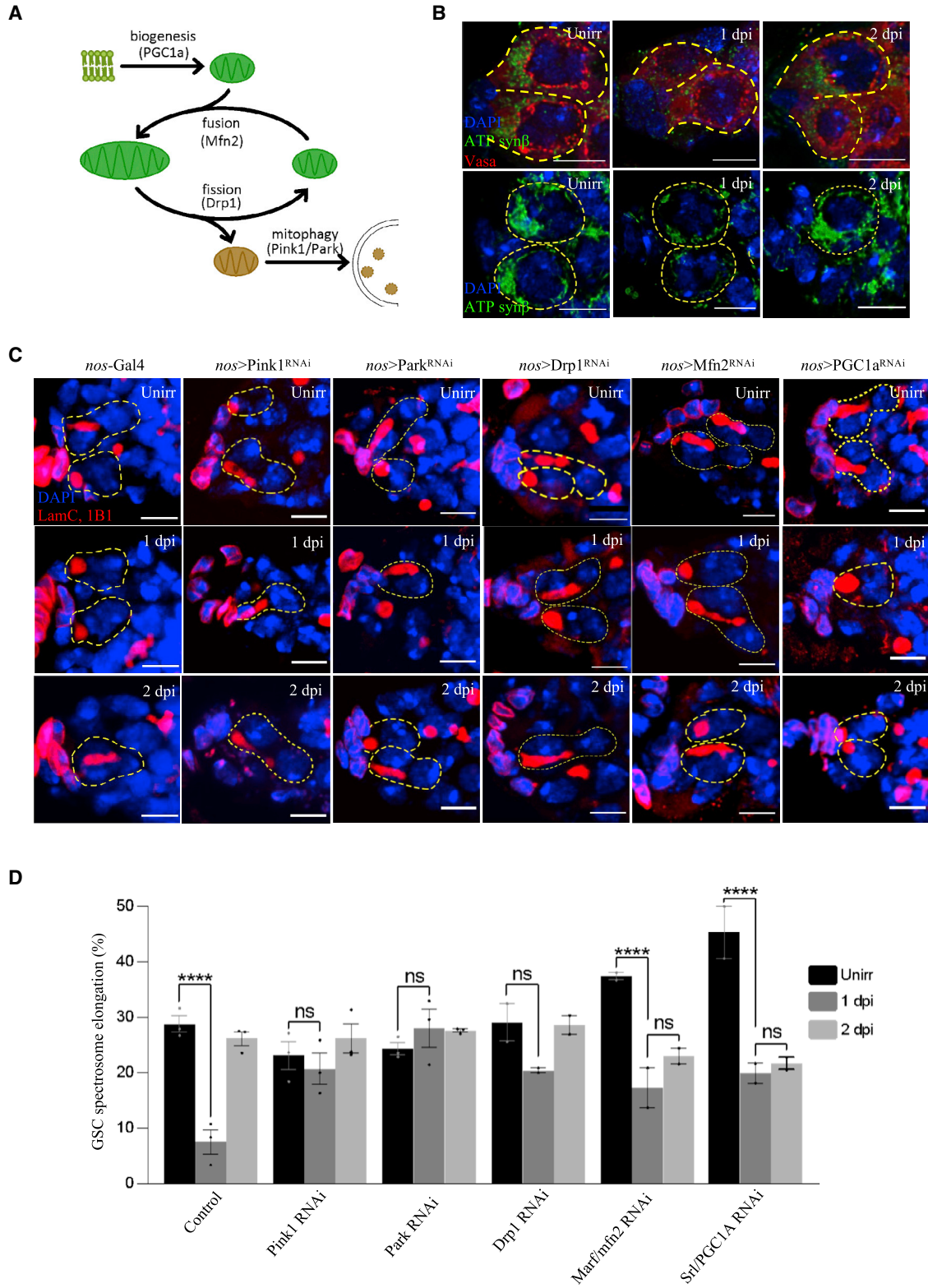
(B) Schematic of known and hypothesized elements of interplay between autophagy and mTORC1.

(C) Immunofluorescence images of GSCs with respective overexpression or knockout of core components of autophagy proteins stained with 1B1 (red, spectroscopomes/fusomes), LamC (red, CpCs and TFs), and DAPI (blue, nuclei). Dotted circle represents GSC (scale bars, 5 μ m).

(D) Percentage of GSCs showing spectroscopome elongation. * $p \leq 0.05$ and *** $p \leq 0.001$.

defective, can result in disease states (Sun et al., 2016). We tested if the mTOR pathway in GSCs has the capacity to control mitophagy, as seen in another context (de la Cruz López et al., 2019). While the mitochondrial network of unirradiated WT GSCs was relatively fused and reticular, with increased mitochondrial density at the anterior end of the GSCs (Figures 3B and 5F) (Lieber et al., 2019; Cox and Spradling, 2003; Wang et al., 2016), at 1 dpi, most of the mitochondria were abnormal, 29% of GSCs with significantly decreased mitochondrial content (Figures 3B, 5A, 5F, and 5G). This decrease in mitochondrial content is dependent on autophagy, since Atg3 mutant GSCs display a normal anterior mitochondrial pattern at 1 dpi (Figures 5F, 5G,

and S3M). Finally, at 2 dpi, the mitochondria returned to a more fused, anterior network, like the mitochondria of unirradiated GSCs (Figures 3B, 5A, 5F, and 5G). We show that Tsc1 RNAi mutant GSCs that lack quiescence (Figures 1F and 1G) also lack mitochondrial reduction at 1 dpi (Figures 5F, 5G, and S3L). These data reveal that GSC mitochondrial degradation and biogenesis coincide with mTOR-dependent entry into and exit from quiescence. This finding is strikingly like that in yeast, wherein proliferating yeast cells contain a tubular meshwork of mitochondria, while quiescent yeast cells have peripheral, fragmented mitochondria (Laporte et al., 2018), suggesting that mitochondrial morphology controls and/or responds to cell



(legend on next page)



proliferation. We tested this hypothesis in stem cells by analyzing IR-induced quiescence in KD of the *Drosophila* mitochondrial proteins, Pink1 and Parkin.

The Parkinson's disease genes Pink1 and Parkin mediate mitochondrial quality control mechanisms that culminate in the clearance of depolarized or dysfunctional mitochondria (Narendra et al., 2008; Matsuda et al., 2010; Vives-Bauza and Przedborski, 2010). We performed Pink1 and Parkin RNAi KD and found that the GSCs lacking Pink1 did not undergo mitochondrial degradation observed with WT GSCs at 1 dpi (Figures 5B, 5F, and 5G), arguing that mitochondria in normal GSCs after insult undergo mitophagy that requires Pink1 kinase activity. Furthermore, while the unirradiated Pink1 and Parkin KD GSCs divide at rates comparable to those of their WT counterparts (Figures 3C and 3D), Pink1 and Parkin KD GSCs still divide at 1 dpi (21% and 28%), failing to enter quiescence (Figures 3C and 3D). Using *nos>mCherry-Atg8a*, we further showed that Pink1-mediated mitophagy was downstream of IR-induced autophagy in GSCs; although Pink1 KD GSCs lacked mitophagy at 1 dpi, they still contained a significant increase in red puncta (Figure S3N). Our findings demonstrate that Pink1 and Parkin-mediated mitophagy is required for GSC IR-induced quiescence.

We also analyzed the canonical regulators of mitochondrial dynamics in GSC quiescence, which are known to interact with the mitophagy receptors Pink1/Parkin (Poole et al., 2010; Deng et al., 2008a, 2008b). We first analyzed the GTPase Dynamin-related protein, Drp1, which forms helical oligomers to pinch around the outer mitochondrial membrane and induce fission. Drp1 KD GSCs divided normally (29%) before irradiation but exhibited defects in arresting division at 1 dpi (20.5%) (Figures 3C and 3D), which implicates the role of mitofission (Figure 3A) in the entry into quiescence. Further, depletion of Marf/Mfn2, a GTPase responsible for mitochondrial fusion, showed a higher than normal division rate in unirradiated GSCs, and a reduced division at 1 dpi (>2-fold reduction), but failed to increase division by 2 dpi (Figures 3C and 3D). Similar to Mfn2 KD, mitochondrial biogenesis regulator PGC1 α /srl KD GSCs also divided more than WT controls and significantly reduced division at 1 dpi (>2-fold reduction), but failed to increase division at 2 dpi (Figures 3C and 3D). These data show that PGC1 α /srl KD GSCs un-

dergo normal mitochondrial degradation at 1 dpi but fail to return to a more normal anterior accumulation of mitochondria at 2 dpi (Figures 5D, 5F, and 5G). In line with these data, in the fly FUCCI line, the black GSCs marked for quiescence at 1 dpi showed a significant reduction in mitochondria (Figure S1F). These data show that in GSCs, mitochondrial fission and mitophagy are required for the entry into quiescence, and mitochondrial fusion and biogenesis are required for the exit from quiescence.

Epigenetic modifiers are required for GSC entry into and exit from quiescence

The epigenome has been previously shown to be regulated by mitochondrial metabolites, and epigenomic changes have been identified in quiescent stem cell states (van Velthoven and Rando, 2019; Cho et al., 2019; Hussein et al., 2020; Somasundaram et al., 2020; Hu et al., 2020; Martínez-Reyes and Chandel, 2020; Moody et al., 2017; Levy et al., 2022). We now show that KD of the PRC1 (Pc/CBX and Sce/RING1) or PRC2 (Jarid2, Su(z)12, E(z), and Jing) components in GSCs abolishes the normal IR-induced cell-cycle block at 1 dpi, suggesting that these repressive epigenomic modifiers are required for entry into GSC quiescence (Figures 4A, 4B, and S3). Interestingly, some transcriptionally activating epigenetic modifiers were also required for quiescence entry, such as H3K10 kinase, Jil1 (Deng et al., 2008a, 2008b); H3K79 methyltransferase, Gpp/DOT1L; and H3K4me2/3 methyltransferase, Set1 (Hallson et al., 2012) (Figures S3A–S3J and Table S1), suggesting that quiescence requires specific transcriptionally activating modifications. Additional enzymes responsible for recognizing DNA damage, γ -H2Av kinase and mei-41/ATR, are required for quiescence (Figures S3C and S3J and Table S1).

Conversely, we found another class of epigenetic modifiers that seem to be essential for the exit from quiescence. RNAi KD of Utx, an H3K27me3 demethylase, prevents GSCs from exiting quiescence (Figures 4A and 4B). An additional histone modifier, H3K4me1 methyltransferase Trx (Tie et al., 2014), also regulates GSC exit from quiescence (Figures 4A and 4B). Curiously, rhi, a piRNA pathway component and member of the heterochromatin protein 1 (HP1) family (Klattenhoff et al., 2009), likely regulates various aspects of GSC homeostasis and quiescence, as rhi RNAi KD causes low baseline division before irradiation

Figure 3. Mitochondrial remodeling events are required for proper coordination of quiescence

- (A) Current model of mitochondria life cycle based on current literature.
 (B) Representative confocal microscopy images of control GSCs from unirradiated, 1 dpi, and 2 dpi germaria stained with VASA (red), ATP synthase β subunit (ATPsyn β) (green, mitochondria), and DAPI (blue, nuclei) (top) or only ATPsyn β and DAPI (bottom). Scale bars, 5 μ m.
 (C) Representative confocal microscopy images of RNAi KD of mitochondrial fission (Drp1) and mitophagy (Pink1/Park) and mitochondrial fusion (Mfn2) and biogenesis (PGC1 α) genes from unirradiated, 1 dpi, and 2 dpi germaria stained with 1B1 (red, spectroosomes/fusomes), LamC (red, CpCs and TFs), and DAPI (blue, nuclei). Dotted circle represents GSC (scale bars, 5 μ m).
 (D) Percentage of GSCs showing spectroosome elongation. ****p \leq 0.0001.

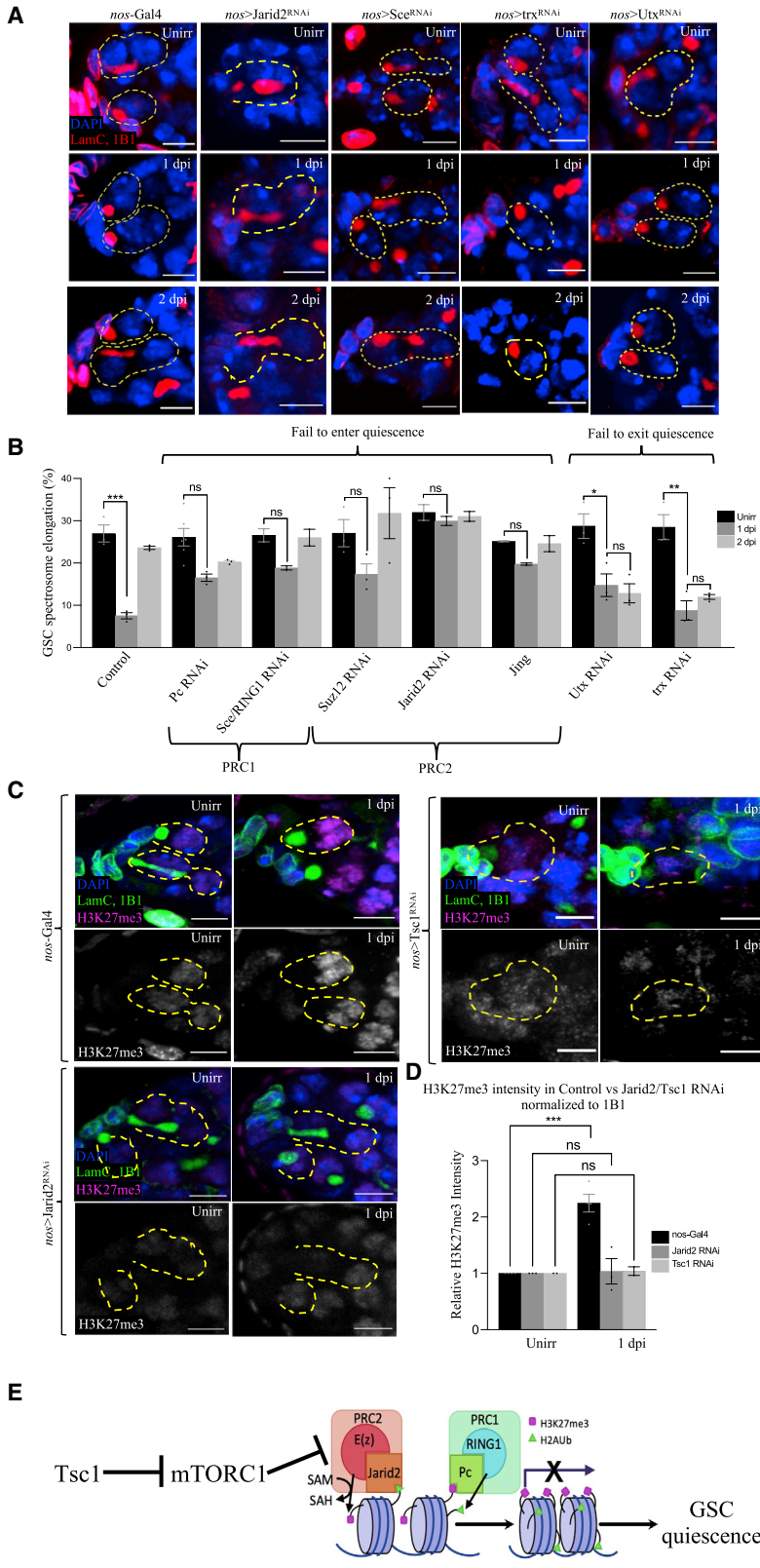


Figure 4. Epigenetic proteins also regulate GSC quiescence

(A) Representative confocal microscopy images of RNAi KD of various epigenetic regulatory genes from unirradiated, 1 dpi, and 2 dpi germaria stained with 1B1 (red, spectrosomes/fusomes), LamC (red, CpCs and TFs), and DAPI (blue, nuclei). Dotted circle represents GSC (scale bars, 5 μ m).

(B) Percentage of GSCs showing spectrosome elongation.

(C) Representative confocal microscopy images of control, Jard2-RNAi, and Tsc1-RNAi GSCs from unirradiated, 1 dpi, and 2 dpi germaria stained with LamC (green, CpCs and TFs), 1B1 (green, spectrosomes/fusomes), H3K27me3 (magenta), and DAPI (blue, nuclei). Dotted circle represents GSC (scale bars, 5 μ m).

(D) Quantification of relative fluorescence intensity of H3K27me3 normalized to 1B1 intensity in control GSCs and Jard2 RNAi GSCs, unirradiated and at 1 dpi. (E) Upon irradiation, the canonical roles of PRC1 and PRC2 in epigenetic regulation during quiescence are shown. PRC2 binds to DNA by Jarid2, while E(z) consumes SAM to methylate H3K27, leading to transcriptional repression. PRC1 then binds to and recognizes existing H3K27me3 marks through CBX, and then catalyzes monoubiquitination of H2A, which further represses transcription and hence leads to quiescence. * $p \leq 0.05$, ** $p \leq 0.01$, and *** $p \leq 0.001$.

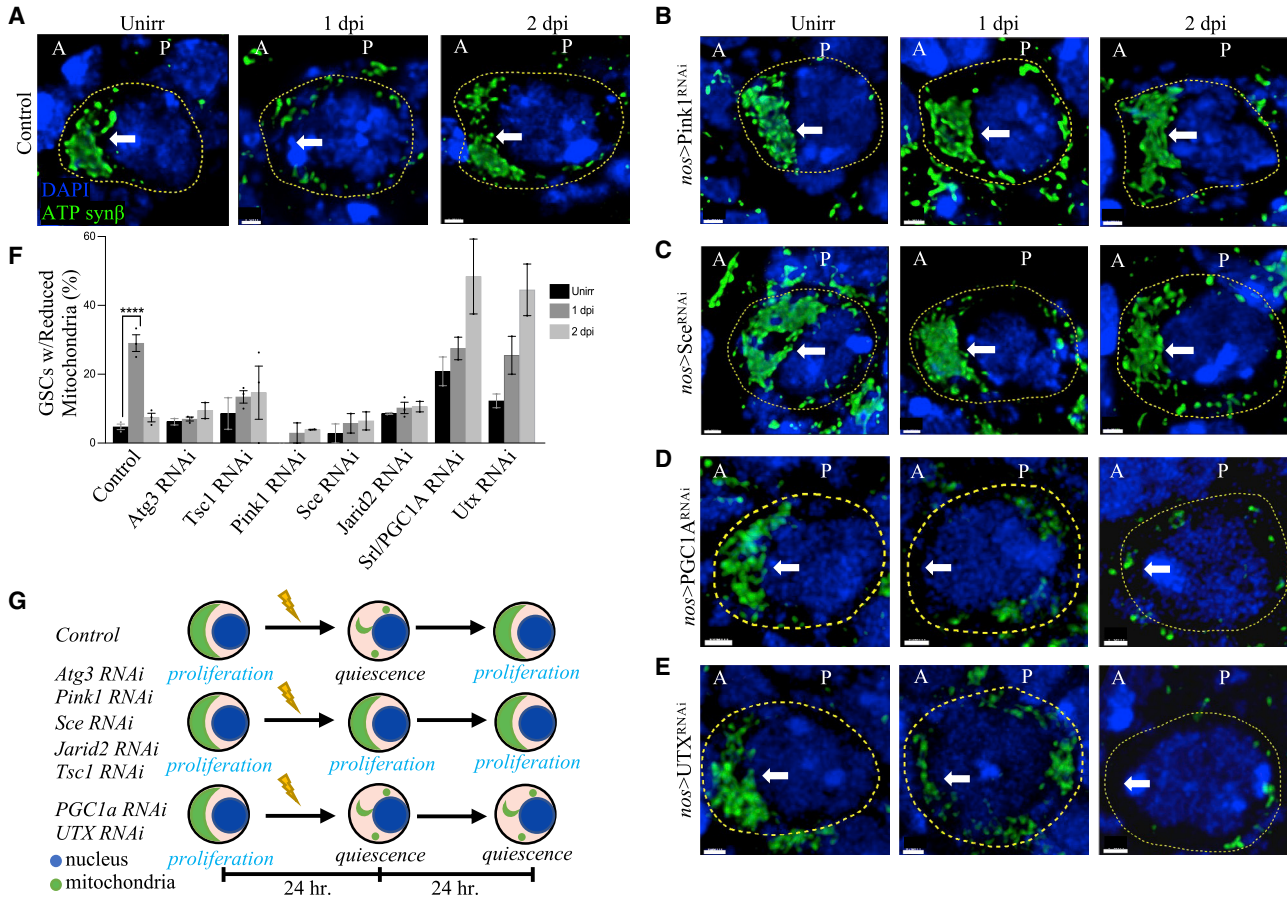


Figure 5. Mitophagy-dependent quiescence is mediated by PRC1

(A–E) Representative 3D reconstructed confocal microscopy images of GSCs and their respective RNAi KD line when unirradiated and at 1 and 2 dpi, stained with DAPI (blue, nuclei) and ATPsynβ (green, mitochondria) (“A” denotes anterior side, and “P” denotes the posterior side of the GSC). Arrow points to the area of interest, where mitochondria are typically clustered (scale bars, 1 μm).

(F) Quantification of incidence of reduced mitochondria where clustered mitochondria are not present in GSCs. Images from Figures S3K–S3M were used to generate this quantification.

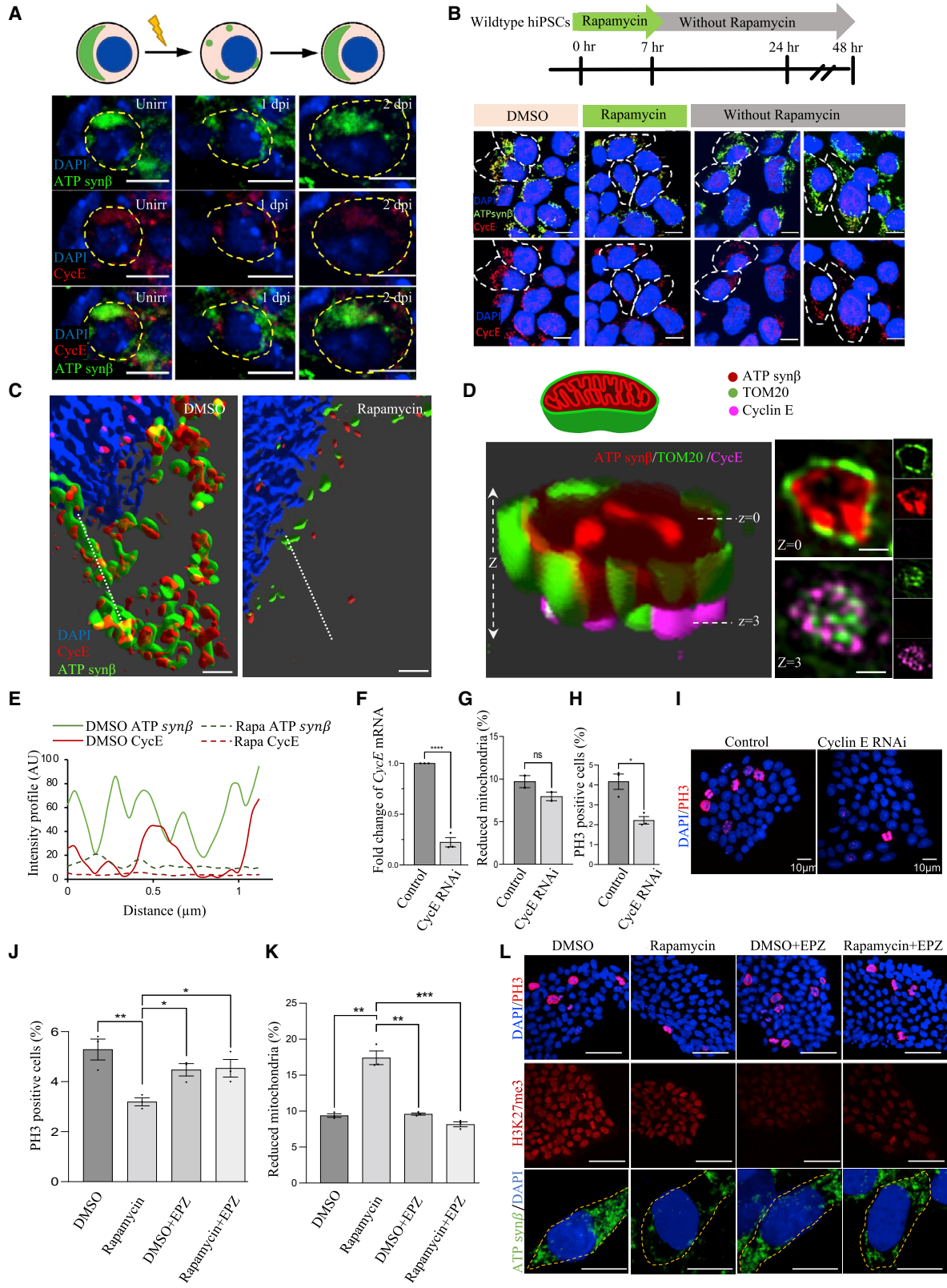
(G) Proposed model by which mitochondria population acts as a checkpoint for the cell-cycle state of GSC. Blue represents nucleus and green represents mitochondria. ****p ≤ 0.0001.

and impairs quiescence entry and exit at 1 and 2 dpi, respectively (Figures S3B and S3J and Table S1). We confirmed PRC1/2 activity in WT 1 dpi GSC nuclei by detecting a significant increase in H3K27me3 intensity compared with unirradiated nuclei (Figures 4C and 4D). In contrast, KD of the PRC2 component Jarid2, or mTOR regulator Tsc1, showed no significant difference in H3K27me3 levels at 1 dpi (Figures 4C and 4D). These data show that mTOR acts upstream of PRC1/PRC2 epigenetic modifiers that are required for GSC quiescence (Figure 4E).

Mitophagy-dependent quiescence is under dynamic epigenetic control

To test the relationship between mTOR, mitophagy, and epigenetic control of GSC IR-induced quiescence, we

stained GSCs with ATPsynβ to analyze mitochondrial pattern and morphology in Tsc1, Pink1, Sce, PGC1/srl, and Utx RNAi mutants (Figures 5A–5F and S3K–S3L). As discussed above, at 1 dpi, the anterior mitochondrial network is lost in most of the WT GSCs, and the GSC ratio with dramatically reduced mitochondria is significantly increased. Using the fly FUCCI system we show that the observed mitochondrial reduction after insult occurs during the G0 stage of cell cycle (Figure S1F). The mitochondria morphology and pattern at 2 dpi are similar to those of unirradiated, representing exit from quiescence (Figures 5A, 5F, 5G, and S3K). In contrast, Tsc1 and Pink1 KD GSCs, which fail to enter quiescence after insult (Figures 1E, 1G, 3C, and 3D) showed the fewest changes in the mitochondrial network at 1 dpi (3%) (Figures 5B,



(legend on next page)



5F, S3K, and S3L), consistent with mTOR action upstream of mitophagy. Interestingly, epigenetic regulator *Sce*/RING1 KD GSCs, which fail to enter quiescence after insult (Figures 4A and 4B), also display low mitochondrial reduction (6%) at 1 dpi (Figures 5C, 5F, and S3K). Furthermore, *Jarid2* RNAi mutants failed to detect IR-induced autophagy (Figure S3N). In contrast, *PGC1* and *Utx* RNAi mutants continued to display segmented and highly reduced mitochondria at 2 dpi (Figures 5D–5F). These data suggest that PRC1/PRC2 and H3K27me3 demethylation are required for mitochondrial regulated quiescence and that the PRC1/PRC2-based epigenetic modifications act upstream of the mitophagy (Figure 5G).

Cyclin E localized to the mitochondria is degraded upon genotoxic or chemical insult in GSCs and hiPSCs

Since female *Drosophila* GSC division does not rely heavily on mitochondrial ATP (Teixeira et al., 2015), we tested the hypothesis that the mitochondria play a more direct role in cell-cycle progression. Cyclin E, a G1-S regulator, has been reported to be targeted for degradation by ubiquitination by Parkin (Staropoli et al., 2003), the E3 ubiquitin ligase required for mitophagy and GSC quiescence (Figures 3C and 3D). Furthermore, Parkin mutations are associated with increased Cyclin E in both cancer and Parkinson's neu-

rons (Veeriah et al., 2010). This Parkin ubiquitination activity on Cyclin E is regulated by a serine/threonine kinase, Pink1 (Ejma et al., 2020). While Parkin is involved in mitophagy and ubiquitin-dependent degradation of Cyclin E, the connection between them remains unclear. Since recent work has observed some Cyclin E co-localization with the mitochondria in both flies and mammals (Parker et al., 2015; Spurlock et al., 2020), we tested the hypothesis that Pink1-activated Parkin will be localized to mitochondria, where it initiates Cyclin E degradation and mitophagy, resulting in quiescence.

In *Drosophila*, unirradiated GSCs show striking co-localization of Cyclin E with the anteriorly localized, fused mitochondrial network (Figure 6A; Lieber et al., 2019; Cox and Spradling, 2003). However, at 1 dpi, the GSCs show a dramatic loss of quantity and anterior localization of both Cyclin E and mitochondria, while at 2 dpi, Cyclin E is once again observed co-localizing with the mitochondria, which are fused and anteriorly localized (Figures 6A and S3P). These data confirm that the mitochondria likely harbor a pool of Cyclin E in GSCs and support the hypothesis that the mitochondrial content dictates cell-cycle progression after insult by regulating the Cyclin E availability for G1-S transition.

To further understand whether the mTOR-regulated, p21 independent, irradiation-induced *Drosophila* GSC

Figure 6. Pool of cyclin E is observed on mitochondria in GSCs and hiPSCs

- (A) Representative confocal microscopy images of *Drosophila* GSCs from unirradiated, 1 dpi, and 2 dpi germaria stained with ATPsyn β (mitochondria, green), cyclin E (red), and DAPI (blue) with cartoon schematic above (scale bars, 5 μ m).
- (B) Model shows the experimental design. Representative confocal microscopy images of WT hiPSCs treated with either vehicle control (DMSO) or rapamycin (2 μ M) and pulse-chase stained with ATPsyn β (mitochondria, green), cyclin E (red), and DAPI (blue) (scale bars, 10 μ m). hiPSCs shows reduction in both mitochondrial and cyclin E density compared with vehicle control after 7 h of 2 μ M rapamycin treatment. Both mitochondria and cyclin E densities increase after 24 and 48 h post rapamycin treatment. Gray dashes represent the boundary of the cells of interest.
- (C) Representative 3D-reconstructed OMX super-resolution microscopy images of WTC cells treated with vehicle control (DMSO) or 2 μ M rapamycin for 24 h and stained with ATPsyn β (green), cyclin E (red), and DAPI (blue). The white dotted line was used to quantify the intensity profile in (E) (scale bars, 0.5 μ m).
- (D) A super-resolution 3D reconstruction of a mitochondrion in Tom20-GFP-expressing WTC, stained for ATPsyn β (red), GFP (green), and cyclin E (magenta). On the right, the two sections $z = 0$ and $z = 3$ show the mid-section and bottom of the mitochondrion (scale bars, 0.5 μ m).
- (E) Intensity profile of ATPsyn β (green) and Cyclin E (red) in DMSO (solid line) and rapamycin (dotted line). The images in (C) were used to quantify the plot profile.
- (F) Fold change of Cyclin E analyzed in qPCR after knocking down Cyclin E with siRNA for 72 h.
- (G) Percentage of cells with reduced mitochondria in control or Cyclin E siRNA for 72 h, $n = 3$, number of cells analyzed per condition >500.
- (H) Percentage of cells positive for PH3 in control or Cyclin E siRNA for 72 h, $n = 3$, number of cells analyzed per condition >500.
- (I) Representative confocal microscopy images of wild-type hiPSCs transfected with either control or cyclin E siRNA for 72 h. DAPI is blue, PH3 is red (scale bars, 10 μ m).
- (J) Percentage of cells positive for PH3 in DMSO, 2 μ M rapamycin, EPZ-6438, and rapamycin + EPZ-6438 for 24 h, $n = 3$, number of cells analyzed per condition >1,000.
- (K) Percentage of cells with reduced mitochondria in DMSO, 2 μ M rapamycin, EPZ-6438, and rapamycin + EPZ-6438 for 24 h, $n = 3$, number of cells analyzed per condition >500.
- (L) Representative confocal images of cells treated with DMSO, 2 μ M rapamycin, EPZ-6438, and rapamycin + EPZ-6438 for 24 h. Cells were stained for DAPI (blue), PH3 (red, scale bar, 50 μ m), ATPsyn β (green, scale bar, 10 μ m), and H3K27Me3 (red, scale bars, 50 μ m). (B–E) wild type, WTC. (F–L) control, WTC-Tom20. * $p \leq 0.05$, ** $p \leq 0.01$, *** $p \leq 0.001$, and **** $p \leq 0.0001$.



quiescence is conserved in mammalian stem cells, we irradiated hiPSCs and analyzed if the process resulted in mTOR inhibition (Qi et al., 2009; Zhan et al., 2019). Previous work has shown that phosphorylation and nuclear exit of the transcription factor TFE3 indicate mTOR activity in hiPSCs (Figure S4G; Mathieu et al., 2019). We therefore analyzed TFE3 nuclear localization in hiPSCs before and after irradiation (0.52 Gy of gamma-irradiation). As expected, TFE3 was mainly observed in the cytoplasm in control hiPSCs (Figures S4B and S4C). However, irradiation induced a 6-fold increase in nuclear TFE3 localization (1 dpi), suggesting that irradiation inhibits mTOR (Figure S4B). Concomitantly, irradiation induced a significant reduction in mitochondria in 80% of the hiPSCs (Figure S4A). These data suggest that irradiation inactivates mTOR and induces mitophagy also in hiPSC. Rapamycin treatment (mTOR inhibition) has previously been shown to induce quiescence (a diapause-like state) in pluripotent stem cells (Hussein et al., 2020). We, therefore, treated the hiPSCs with rapamycin as a surrogate of irradiation-induced mTORC1 inhibition and analyzed the effect of mitochondrial dynamics on CycE levels in quiescent hiPSC. We confirmed that rapamycin inhibits mTORC1 in hiPSCs (reduced pS6 within 7 h of treatment; Figure S4E). We found a stronger, but reversible inhibition of mTORC1 if rapamycin treatment was extended to 24 h (pS6 signal returns in 3 days after mTORC1 reactivation (Figures S4E and S4F). Twenty-four hours of rapamycin treatment also promoted significant nuclear localization of TFE3, confirming rapamycin efficiency in our experimental setup (Figure S4G). Importantly, rapamycin treatment resulted in a reversible reduction of epigenetic H4K16Ac marks (Figures S4E and S4F), indicating reduced cellular transcription previously seen in ESC diapause/quiescence (Hussein et al., 2020). These data suggest that hiPSCs can enter reversible quiescence after mTOR inhibition by rapamycin. Importantly, we observed a dramatic co-localization of CycE and mitochondria also in hiPSCs (Figures S4D, S4H, and S4I). The rapamycin-dependent co-localization of CycE and mitochondria was also reversible: while 7 h rapamycin treatment drastically decreased the patterns, after 24–48 h recovery, the mitochondria and CycE co-localization was similar to that of the vehicle controls (Figure 6B). These data confirm that mTORC1 inhibition in hiPSCs degrades both mitochondria and CycE, in a reversible manner.

Using super-resolution microscopy, we observed distinct co-localization of CycE with an outer mitochondrial membrane import receptor subunit, Tom20 (in the same mitochondrial region), but not with ATPsyn β , suggesting that the mitochondrial pool of CycE resides on the outer mitochondrial membrane (OMM) (Figure 6D). Upon rapamycin treatment (2 μ M, 24 h) the mitochondria degraded, with a concomitant reduction in OMM CycE levels (Figures 6C

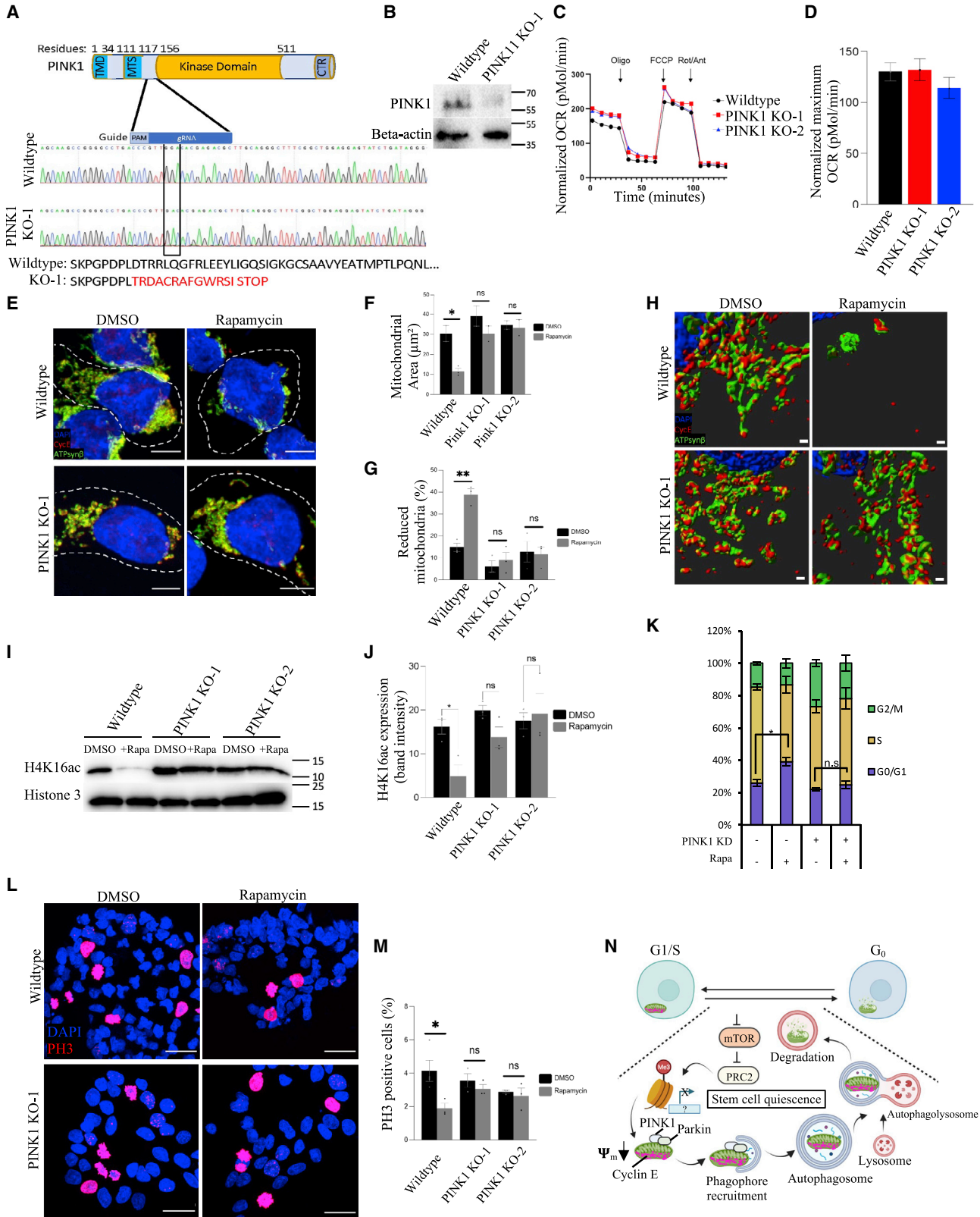
and 6D). The reduction of mitochondrial CycE is proteasome dependent, since it can be reversed by treatment with a proteasome inhibitor (MG132; however, this does not rule out lysosomal degradation) (Figure S4M). To further test if CycE is critical for quiescence in iPSCs, we knocked down CycE (72 h; Figure 6F) and observed a significant decrease in PH3-positive cells, without altering mitochondrial reduction (Figures 6G–6I). This further implies that a reduced level of CycE is directly associated with stem cell entry into quiescence in hiPSCs.

Epigenetic control of hiPSC quiescence

When we treated hiPSCs with rapamycin to inhibit mTOR, and EPZ-6438 to inhibit EZH2, a component of the PRC2 complex, we confirmed PRC2 inhibition by a reduction in H3K27me3 (Figures 6L and S4K). In rapamycin treatment we observed a significant reduction in the number of PH3⁺ cells, showing that rapamycin can induce a quiescence-like cell-cycle block in hiPSCs (Figures 6J and 6L). Further, we found that co-treatment of rapamycin with EPZ-6438 (Figure S4J) prevented hiPSCs from entering mTOR inhibition-dependent quiescence (Figures 6J and 6L). These data suggest that PRC2-mediated gene repression is essential for quiescence in hiPSCs and acts downstream of mTOR regulation. The control hiPSCs showed a significant increase in mitochondrial reduction in rapamycin-treated samples, while co-treatment of rapamycin and EPZ-6438 showed a lack of mitochondrial reduction (Figures 6K and 6L). This suggests that the state of quiescence induced through mTORC1 inhibition in hiPSCs is mediated by repressive histone marks, H3K27me3, which are upstream of mitochondrial degradation/fragmentation.

PINK1-mediated mitophagy dictates quiescence through cyclin E in hiPSCs

To further investigate the role of mitophagy in regulating the stability of CycE, we generated hiPSC lines with CRISPR-Cas9-induced mutations in the mitochondrial serine/threonine protein kinase PINK1. PINK1 contains an N-terminal mitochondrial localization sequence, a transmembrane sequence, a Ser/Thr kinase domain, and a C-terminal regulatory domain (Schubert et al., 2017) (Figure 7A). We engineered the CRISPR-Cas9 system to induce mutations prior to the kinase domain, thereby eliminating the PINK1 kinase activity (Figure 7A). We generated CRISPR mutants in two genetic backgrounds in which 90% of the cells generated had indels near the PAM region, resulting in dramatically reduced levels of PINK1 protein (Figures S5A and S5B). In addition to the KD, we generated two homozygous knockout lines with one base deletion that caused a frameshift and led to an early stop codon (Figures 7A, 7B, and S5A). The PINK1 knockout lines



(legend on next page)



remain pluripotent and have the capacity to initiate differentiation into all three lineages similar to the WT iPSCs (Figures S5C–S5E). To characterize the metabolic profile of PINK1 knockout hiPSCs, we performed a mitostress assay to measure oxygen consumption rate (OCR) to determine the level of mitochondrial respiration using a Seahorse flux analyzer (Hussein et al., 2020; Sperber et al., 2015; Zhou et al., 2012; Miklas et al., 2019). The OCRs in response to FCCP (an uncoupling agent of mitochondrial oxidative phosphorylation) between WT and PINK1 knockout cells were indistinguishable (Figures 7C and 7D). We conclude that PINK1 KO cells are pluripotent and have a characteristic hiPSC metabolism.

We treated both control hiPSCs and PINK1 KD hiPSCs, as well as the two homozygous knockout hiPSCs, with rapamycin or vehicle for 24 h. As before (Figures S6B–S6D), control hiPSCs showed dense, fused mitochondrial networks, with only ~10% of cells exhibiting reduced mitochondria and CycE, but after 24 h of treatment with 2 μ M rapamycin, mitochondrial and CycE levels were reduced significantly (Figures 7E–7H and S6A–S6G). In contrast, PINK1 mutant hiPSCs showed little to no mitochondrial or CycE reduction, regardless of whether they were treated with DMSO or rapamycin, suggesting that PINK1/Parkin-mediated mitophagy is required for OMM CycE degradation (Figures 7E–7H and S6A–S6I).

We show that rapamycin treatment downregulates H4K16Ac levels in WT, but not in PINK1 knockout cells (Figures 7I and 7J), indicating that PINK-dependent mitophagy is required for a transcriptionally silent iPSC quiescent stage. Moreover, using the PH3⁺ mark to assess hiPSC proliferation, we found that rapamycin reduces cell division by up to 50% in control, but not in PINK1 mutant, hiPSCs (Figures 7L, 7M, S7A–S7D, and S7F). We also show that hiPSCs treated with vehicle (DMSO) for 24 h show a portion of cells in G0/G1 (25.5%), a large portion in S (58.4%), and the remainder in G2/M (14.7%) (Figures 7K and S7G). Conversely, after 24 h of rapamycin treatment, hiPSCs show significant G0/G1 arrest (38.7%), consistent with the idea that rapamycin and mTOR inhibition induces a diapause-like state of cellular quiescence in human hiPSCs. However, rapamycin-treated PINK1 mutant hiPSCs show no significant difference compared with vehicle-treated PINK1 mutant hiPSCs (Figures 7K and S7G). The inability of PINK1 mutant hiPSCs to arrest in G0 is consistent with mitophagy reducing CycE and therefore G1-S transition. These data indicate that hiPSCs, like *Drosophila* GSCs, utilize a non-canonical method of regulating the available reservoir of CycE via PINK1/PARKIN-mediated mitophagy. Together, these findings across stem cell types suggest that diverse stem cells may rely on mitochondrial count

Figure 7. Mitophagy in hiPSCs controls both mitochondrial cyclin E and cell cycle

- (A) Pink1 structure with guide RNA location indicated and DNA sequencing chromatogram comparing wild-type Pink1 to mutant Pink1, showing a mixed pool of mutants and a loss of the wild-type sequence.
- (B) Western blot showing Pink1 protein knocked out.
- (C and D) Representative trace of OCR changes in response to oligomycin, FCCP, and rotenone/antimycin is shown under a MitoStress protocol (C). Pink1 KO cells show similar mitochondrial respiration pattern compared with wild-type Pink1 (D).
- (E) Representative confocal microscopy images of wild-type or Pink1 mutant cells treated with either vehicle control (DMSO) or rapamycin (2 μ M) and stained with DAPI (blue), CycE (red), and ATPsyn β (mitochondria, green) (scale bars, 5 μ m).
- (F and G) Quantification of (F) area of mitochondria and (G) mitochondrial degradation in wild type vs. Pink1 mutant treated with either vehicle control (DMSO) or rapamycin (2 μ M). Following are the total numbers of cells quantified (n) for wild-type and Pink1-KO cells for DMSO- and rapamycin-treated cells, respectively: wild type (without cyclin E stain), 618, 518; wild type (with cyclin E stain), 512, 414; Pink1-KO cells (without cyclin E stain), 616, 701; wild type (with cyclin E stain), 502, 569.
- (H) Representative 3D reconstructed OMX super-resolution microscopy images of wild-type or Pink1 mutant cells stained with DAPI (blue), CycE (red), and ATPsyn β (mitochondria, green) (scale bars, 0.2 μ m).
- (I) Representative western blot analysis of wild type, Pink1 KO-1, and Pink1 KO-2 treated with DMSO or 2 μ M rapamycin for 24 h and blotted with H4K16Ac and histone 3 as a loading control.
- (J) H4K16Ac quantification of the western blot in (I).
- (K) Quantification of fluorescence-activated cell sorting (FACS) analysis of cell cycle by propidium iodide staining in wild type or Pink1KD treated with DMSO or rapamycin (2 μ M).
- (L) Representative confocal microscopy images of wild-type or Pink1 mutant cells treated with either vehicle control (DMSO) or rapamycin (2 μ M) and stained with DAPI (blue) and PH3 (proliferating cell nuclei, red) (scale bars, 15 μ m).
- (M) Quantification of PH3 incidence in wild type vs. Pink1 mutant treated with either vehicle control (DMSO) or rapamycin (2 μ M). Following are the total numbers of cells quantified (n) for wild type and Pink1-KO for DMSO- and rapamycin-treated cells, respectively: wild type, 3439, 2760; Pink1-KO, 3162, 3184.
- (N) Model of proposed mechanism in which mitochondria can normally stabilize CycE and promote G1-S transition, while mitophagy induction will reduce CycE—perhaps through direct ubiquitination by Parkin—and keep the stem cells in quiescence/G0. (A–J, M–L) Wild type, WTC-Tom20; (K) wild type, WTC. *p \leq 0.05 and **p \leq 0.01.



to regulate available CycE and, consequently, stem cell quiescence.

DISCUSSION

In this study, we show that the commencement of quiescence in irradiated *Drosophila* GSCs and hiPSCs relies on the quantity of mitochondria (Figure 7N). We show that a failure in mitochondrial degradation abolishes quiescence, allowing a continuous cell cycle, whereas a failure in mitochondrial biogenesis or fusion impairs the exit from quiescence. Our data further suggest that mitochondrial quantity is controlled by the metabolic sensor mTORC1-dependent epigenetic regulation by PRC1/2. Predominantly, our research suggests that mitochondria mechanistically regulate the cell cycle by serving as a harbor for OMM CycE.

We found that the mTOR-responsive transcription factor Mitf and its downstream targets regulating autophagy are required for quiescence. Although autophagy has been shown to be necessary for stem cell quiescence in some contexts (García-Prat et al., 2016; Ho et al., 2017; Wang et al., 2018) and for proliferation in other contexts (Nagy et al., 2018; Salemi et al., 2012), our data unequivocally show that, in female *Drosophila* GSCs, autophagy is required for quiescence. Further, we report that the mitophagy effectors Pink1 and Parkin, as well as the mitofission protein Drp1, are each necessary for quiescence. Conversely, we found that the mitochondrial biogenesis transcription factor PGC1 α and mitofusion protein Mfn2 are required to properly exit from quiescence. In conclusion, the mitochondrial mass tightly regulates reversible quiescence. Given the cross talk between mitophagy and mitochondrial dynamics (Lieber et al., 2019; Deng et al., 2008a, 2008b; Rana et al., 2017; Gong et al., 2015), it will be interesting to dissect whether mitophagy and mitochondrial fission are independent during quiescence, or if they always function in concert. Importantly, in human hiPSCs, we found that rapamycin-induced quiescence requires mitophagy and its regulator PINK1. In contrast, mTORC1 inhibition in mouse embryonic fibroblasts shows increased mitofusion (Morita et al., 2017). Hence, we conclude that mTORC1-inhibition-dependent mitophagy might be a unique character of stem cells.

We show that mitophagy reduced mitochondrial CycE and increased G0 cell-cycle arrest in both GSCs and hiPSCs. Our finding that CycE decorates the OMM in hiPSCs raises the question of how CycE is trafficked between the OMM and the nucleus. We have identified a distinct mechanism whereby mitophagy destabilizes the critical G1/S cell cycle regulator, CycE, halting the cell cycle. While the CycE canonical regulator Dacapo/p21 can control DNA-damage-

induced p53-dependent checkpoint in G0, p21/Dacapo does not appear to play a role in the GSC insult-induced quiescence (Artoni et al., 2017; Yu et al., 2009). We therefore argue that in stem cells, unexpectedly, the mitochondria quantity may be the primary regulator for CycE and act as a checkpoint for entering and exiting quiescence. It will be important to interrogate which stem cell types can utilize this alternative method of G1/S control, and whether this phenomenon can be leveraged for therapeutic purposes, perhaps utilizing AI-based protein design approach (Cao et al., 2022; Anishchenko et al., 2021).

In satellite stem cells, PcG promotes stemness and self-renewal (Margueron and Reinberg, 2011; Caretti et al., 2004; Bracken et al., 2006; Bianchi et al., 2020). In hematopoietic stem and progenitor cells, the PRC1 component Ring1 is required for self-renewal (Eskeland et al., 2010). Here, we show a novel role for the PcG proteins Pc/CBX8 and Sce/Ring1 of PRC1 as regulators of reversible, injury-induced GSC cell-cycle block. In line with our data, the Pc homolog Cbx7 in African killifish has been recently shown to be required for maintaining diapause (Hu et al., 2020). Furthermore, recent findings suggest that cancer-related irradiation and chemotherapy may lead a class of cancer cells (cancer stem cells, CSCs) to enter a protective, reversible diapause-like state (Dhimolea et al., 2021; Rehman et al., 2021; Hussein et al., 2022). Hence, targeting the PRC1/2 complex (Levy et al., 2022) might force cells to exit diapause-like quiescence in the normal, as well as the cancer, state, guiding CSCs to a proliferative stage amenable to conventional chemotherapies. Future work will be needed to examine whether insult-induced quiescence in GSCs requires Jarid2 via a Polycomb repressive element (PRE)-dependent mechanism like traditional *Drosophila* PcG proteins or via a PRE-independent mechanism like the default mammalian method (DeLuca et al., 2020; Herz et al., 2012; Landeira et al., 2010).

The cornerstone of stem cell quiescence in this study is PINK1/PARKIN-mediated mitophagy, which acts downstream of mTOR-dependent PRC2 complex activity (Figure 7N). It is plausible that the CycE pool associated with mitochondria gets directly ubiquitinated by Parkin, leading to an overall decrease in Cdk2/CycE activity essential for G1/S transition, resulting in a reversible G0 cell-cycle halt (Figure 7N). Future research will reveal whether manipulating mTORC1 signaling and mitochondria quantity could restore regenerative capacity to non-regenerative adult tissues like the heart (Miklas et al., 2022). Furthermore, it will be important to dissect in detail if and how mitochondrial dynamics play a role in GSC age-related senescence, as mitochondria have been shown to play a critical role in senescence in many cell types (Rana et al., 2017; Davalli et al., 2016; Scheckhuber et al., 2007; Chaudhari and Kipreos, 2017; Byrne et al., 2019; Pauklin and



Vallier, 2014; Tai et al., 2017). It will be important to investigate if similar epigenetic regulation of mitochondrial dynamics controls insult-induced quiescence in other stem cell types and whether senescence in aging stem cells can be reversed by altering mitochondrial dynamics.

EXPERIMENTAL PROCEDURES

Resource availability

Corresponding author

Further information and requests for resources and reagents should be directed to and will be fulfilled by the corresponding author, Hannele Ruohola-Baker (hannele@uw.edu).

Materials availability

All unique/stable reagents generated in this study are available from the corresponding author without restriction.

Data and code availability

Description of sample size and raw data are provided in the [supplemental information](#). For further information, please contact the corresponding author.

Fly stocks and culture conditions

Flies were cultured at 25°C on cornmeal-yeast-agar medium supplemented with wet yeast (Artoni et al., 2017; Xing et al., 2015). Information regarding fly stocks is given in the [supplemental experimental procedures](#).

hiPSC culture conditions

The hiPSCs were cultured on Matrigel growth factor-reduced basement membrane matrix (Corning) in mTeSR medium (STEMCELL Technologies). The cells were treated with rapamycin (200 nM–2 μM, Fisher Scientific) or DMSO for indicated periods and thereafter tested for reversion in the absence of rapamycin. To analyze the proteasome function, hiPSCs were treated with 100 nM MG132 (proteasomal inhibitor, Thermo Scientific; cat. no. 508339) for 24 h. Information regarding cell lines is given in the [supplemental experimental procedures](#).

Ionizing radiation treatment in *Drosophila* and hiPSCs

Prior to gamma-irradiation exposure, 2- to 4-day-old flies (5–6 M:15–18 F) were kept on cornmeal-yeast-agar medium augmented with wet yeast for 48 h at 25°C. On the day of irradiation, two-thirds of the females and all males were transferred to empty plastic vials and treated with 50 Gy of gamma-irradiation. More details are provided in the [supplemental experimental procedures](#). For irradiation in hiPSCs, we plated 5×10^4 hiPSCs in Matrigel-coated coverslip in 35 mm culture dishes. After 48 h, the dishes were treated with 0.52 Gy of gamma-irradiation. One day post-insult, the cells were fixed in paraformaldehyde and stained.

OCR measurement using Seahorse cellular flux assay

The Seahorse XF96 extracellular flux analyzer was used to assess mitochondrial function as described (Sperber et al., 2015; Zhou et al., 2012; Miklas et al., 2019). Details are given in the [supplemental experimental procedures](#).

Drosophila and hiPSC immunofluorescence analysis

Fly samples and iPSCs were fixed and stained with different antibodies. Details regarding the immunofluorescence is given in the [supplemental experimental procedures](#).

hiPSC gene knockout and knockdown

Guide RNAs (gRNAs) targeting exon 2 of PINK1 (Table S2) were designed using CRISPOR.org (Concordet and Haeussler, 2018) and inserted into a lentiCRISPR v.2 plasmid containing two expression cassettes, hSpCas9 and the chimeric guide RNA (Shalem et al., 2014; Sanjana et al., 2014) (a gift from Feng Zhang; Addgene plasmid 52961), as done before (Arena et al., 2021). The vector was digested using *BsmBI*, and a pair of annealed oligos were cloned into the single guide RNA scaffold. Sequences for the gRNAs and primers used for sequencing can be found in Tables S2 and S3, respectively.

For CycE KD, a million hiPSCs cells were seeded on a Matrigel-coated dish with mTeSR medium with a mixture of CycE siRNA (Dharmacon ON-target Plus SMARTpool siRNA) (Table S4) and RNAi Max (Invitrogen; 13778-075) prepared in Opti-MEM (Gibco; 51985).

hiPSC transduction and selection

hiPSCs were transduced with lentiCRISPR v.2/gRNA lentiviral particles targeting PINK1 with 4 μg/mL polybrene (Sigma Aldrich). Details are provided in the [supplemental experimental procedures](#).

Trilineage differentiation

We differentiated the WT and PINK1 KO hiPSC lines using a STEMdiff Trilineage Differentiation Kit (STEMCELL Technologies; 05231, 05232, 05233). We performed qPCR for lineage-specific markers using a Human Pluripotent Stem Cell Trilineage Differentiation qPCR array kit (STEMCELL Technologies; 07515) and analyzed their differentiation efficiency using the software www.stemcell.com/qPCRanalysis.

Data and resources availability

Description of sample size, raw data, and additional information on experimental procedures are provided in the [supplemental information](#). For further information, please contact the corresponding author.

SUPPLEMENTAL INFORMATION

Supplemental information can be found online at <https://doi.org/10.1016/j.stemcr.2022.11.004>.

AUTHOR CONTRIBUTIONS

Conceptualization, T.H.T., A.M.H., R.K., J.R.I., J.M., and H.R.-B.; data curation, formal analysis, validation, and investigation, T.H.T., A.M.H., R.K., J.R.I., T.C.C., B.N.N., S. Liu, D.B., S.H., S. Lyons, B.G., J.D., N.B., S.J., D.D.C., and J.M.; methodology, T.H.T., A.M.H., R.K., J.R.I., and T.C.C.; visualization, T.H.T., A.M.H., R.K., J.R.I., S. Lyons, S.H., J.M., N.B., and S.J.; writing – original draft, T.H.T., J.R.I., and H.R.B., writing – review & editing, T.H.T., A.M.H., R.K., J.R.I., S. Liu, J.M., and H.R.-B.; resources, J.M.



and D.D.C.; funding acquisition, H.R.B.; project administration, H.R.B.

ACKNOWLEDGMENTS

We thank Prof. Helena Richardson for kindly providing *Drosophila* CycE antibodies. We thank Filippo Artoni, Arianne Caudal, Ondina Palmeira, Ellen Ward, Xiaosheng Yang, Blair Zhao, and other members of the Ruohola-Baker lab for their stimulating discussion and valuable comments. We thank Jennifer Hesson and Christopher Cavanaugh for their help. We thank the Lynn & Mike Garvey Imaging Core at the University of Washington and the Cell Analysis Facility Flow Cytometry Shared Resource Lab in the Department of Immunology at the University of Washington. This research used the ISCRM Ellison Stem Cell core facility expanded cell line made possible through the Allen Cell Collection, available from Coriell Institute for Medical Research. This work is supported by the Biological Mechanisms of Healthy Aging Training Program (NIH T32AG066574 to A.M.H.) and the Hahn Family and partly by grants from the American Heart Association (19IPL0134760143), Department of Defense (W81XWH2110007) and National Institutes of Health (R01GM097372, R01GM083867, 1P01GM081619, U01HL099997, and U01HL099993 to H.R.-B.).

CONFLICT OF INTERESTS

The authors declare no competing interests.

Received: April 26, 2022

Revised: November 2, 2022

Accepted: November 7, 2022

Published: December 8, 2022

REFERENCES

Anishchenko, I., Pellock, S.J., Chidyausiku, T.M., Ramelot, T.A., Ovchinnikov, S., Hao, J., Bafna, K., Norn, C., Kang, A., Bera, A.K., et al. (2021). De novo protein design by deep network hallucination. *Nature* *600*, 547–552.

Arena, R., Bisogno, S., Gąsior, Ł., Rudnicka, J., Bernhardt, L., Haaf, T., Zacchini, E., Bochenek, M., Fic, K., Bik, E., et al. (2021). Lipid droplets in mammalian eggs are utilized during embryonic diapause. *Proc. Natl. Acad. Sci. USA* *118*. e2018362118.

Artoni, F., Kreipke, R.E., Palmeira, O., Dixon, C., Goldberg, Z., and Ruohola-Baker, H. (2017). Loss of foxo rescues stem cell aging in *Drosophila* germ line. *Elife* *6*, e27842.

Aubrey, B.J., Kelly, G.L., Janic, A., Herold, M.J., and Strasser, A. (2018). How does p53 induce apoptosis and how does this relate to p53-mediated tumour suppression? *Cell Death Differ.* *25*, 104–113.

Bianchi, A., Mozzetta, C., Pegoli, G., Lucini, F., Valsoni, S., Rosti, V., Petrini, C., Cortesi, A., Gregoret, F., Antonelli, L., et al. (2020). Dysfunctional polycomb transcriptional repression contributes to lamin A/C-dependent muscular dystrophy. *J Clin Invest* *130*, 2408–2421.

Bouché, V., Espinosa, A.P., Leone, L., Sardiello, M., Ballabio, A., and Botas, J. (2016). *Drosophila* Mitf regulates the V-ATPase and the lysosomal-autophagic pathway. *Autophagy* *12*, 484–498.

Bracken, A.P., Dietrich, N., Pasini, D., Hansen, K.H., and Helin, K. (2006). Genome-wide mapping of Polycomb target genes unravels their roles in cell fate transitions. *Genes Dev.* *20*, 1123–1136.

Bulut-Karslioglu, A., Biechele, S., Jin, H., Macrae, T.A., Hejna, M., Gertsenstein, M., Song, J.S., and Ramalho-Santos, M. (2016). Inhibition of mTOR induces a paused pluripotent state. *Nature* *540*, 119–123.

Byrne, J.J., Soh, M.S., Chandhok, G., Vijayaraghavan, T., Teoh, J.S., Crawford, S., Cobham, A.E., Yapa, N.M.B., Mirth, C.K., and Neumann, B. (2019). Disruption of mitochondrial dynamics affects behaviour and lifespan in *Caenorhabditis elegans*. *Cell. Mol. Life Sci.* *76*, 1967–1985.

Cao, L., Coventry, B., Goreshnik, I., Huang, B., Sheffler, W., Park, J.S.W., and Jude, K.M. (2022). Design of protein-binding proteins from the target structure alone. *Nature* *605*, 551–560.

Caretti, G., Di Padova, M., Micales, B., Lyons, G.E., and Sartorelli, V. (2004). The Polycomb Ezh2 methyltransferase regulates muscle gene expression and skeletal muscle differentiation. *Genes Dev.* *18*, 2627–2638.

Chakravarti, A., Thirimanne, H.N., Brown, S., and Calvi, B.R. (2022). Isoforms have overlapping and distinct functions in germline genome integrity and oocyte quality control. *Elife* *11*, e61389.

Chaudhari, S.N., and Kipreos, E.T. (2017). Increased mitochondrial fusion allows the survival of older animals in diverse *C. elegans* longevity pathways. *Nat. Commun.* *8*, 182.

Cho, I.J., Lui, P.P., Obajdin, J., Riccio, F., Stroukov, W., Willis, T.L., Spagnoli, F., and Watt, F.M. (2019). Mechanisms, hallmarks, and implications of stem cell quiescence. *Stem Cell Rep.* *12*, 1190–1200.

Concordet, J.P., and Haeussler, M. (2018). CRISPOR: intuitive guide selection for CRISPR/Cas9 genome editing experiments and screens. *Nucleic Acids Res.* *46*, W242–W245.

Cox, R.T., and Spradling, A.C. (2003). A Balbiani body and the fusome mediate mitochondrial inheritance during *Drosophila* oogenesis. *Development* *130*, 1579–1590.

Davalli, P., Mitic, T., Caporali, A., Lauriola, A., and D’Arca, D. (2016). ROS, cell senescence, and novel molecular mechanisms in aging and age-related diseases. *Oxid. Med. Cell. Longev.* *2016*, 3565127.

DeLuca, S.Z., Ghildiyal, M., Pang, L.Y., and Spradling, A.C. (2020). Differentiating *Drosophila* female germ cells initiate Polycomb silencing by regulating PRC2-interacting proteins. *Elife* *9*, e56922.

Deng, H., Bao, X., Cai, W., Blacketer, M.J., Belmont, A.S., Girton, J., Johansen, J., and Johansen, K.M. (2008a). Ectopic histone H3S10 phosphorylation causes chromatin structure remodeling in *Drosophila*. *Development* *135*, 699–705.

de la Cruz López, K.G., Toledo Guzmán, M.E., Sánchez, E.O., and García Carrancá, A. (2019). mTORC1 as a regulator of mitochondrial functions and a therapeutic target in cancer. *Front. Oncol.* *9*, 1373.

Deng, H., Dodson, M.W., Huang, H., and Guo, M. (2008b). The Parkinson’s disease genes pink1 and parkin promote mitochondrial fission and/or inhibit fusion in *Drosophila*. *Proc. Natl. Acad. Sci. USA* *105*, 14503–14508.



- Dhimolea, E., de Matos Simoes, R., Kansara, D., Al'Khafaji, A., Bouyssou, J., Weng, X., Sharma, S., Raja, J., Awate, P., Shirasaki, R., et al. (2021). An embryonic diapause-like adaptation with suppressed myc activity enables tumor treatment persistence. *Cancer Cell* 39, 240–256.e11.
- Ejma, M., Madetko, N., Brzecka, A., Guranski, K., Alster, P., Misiuk-Hojło, M., Somasundaram, S.G., Kirkland, C.E., and Aliev, G. (2020). The links between Parkinson's disease and cancer. *Biomedicines* 8, E416.
- Eskeland, R., Leeb, M., Grimes, G.R., Kress, C., Boyle, S., Sproul, D., Gilbert, N., Fan, Y., Skoultchi, A.I., Wutz, A., and Bickmore, W.A. (2010). Ring1B compacts chromatin structure and represses gene expression independent of histone ubiquitination. *Mol. Cell* 38, 452–464.
- García-Prat, L., Martínez-Vicente, M., Perdiguero, E., Ortet, L., Rodríguez-Ubrea, J., Rebollo, E., Ruiz-Bonilla, V., Gutarra, S., Ballestar, E., Serrano, A.L., et al. (2016). Autophagy maintains stemness by preventing senescence. *Nature* 529, 37–42.
- Goding, C.R., and Arnheiter, H. (2019). MITF—the first 25 years. *Genes Dev.* 33, 983–1007.
- Gong, G., Song, M., Csordas, G., Kelly, D.P., Matkovich, S.J., and Dorn, G.W. (2015). Parkin-mediated mitophagy directs perinatal cardiac metabolic maturation in mice. *Science* 350, aad2459.
- Hallson, G., Hollebakk, R.E., Li, T., Syrzycka, M., Kim, I., Cotsworth, S., Fitzpatrick, K.A., Sinclair, D.A.R., and Honda, B.M. (2012). dSet1 is the main H3K4 di- and tri-methyltransferase throughout *Drosophila* development. *Genetics* 190, 91–100.
- He, F., Borchers, W., Song, T., Wei, X., Das, M., Chen, L., Daughdrill, G.W., and Chen, J. (2019). Interaction between p53 N terminus and core domain regulates specific and nonspecific DNA binding. *Proc. Natl. Acad. Sci. USA* 116, 8859–8868.
- Herz, H.M., Mohan, M., Garrett, A.S., Miller, C., Casto, D., Zhang, Y., Seidel, C., Haug, J.S., Florens, L., Washburn, M.P., et al. (2012). Polycomb repressive complex 2-dependent and -independent functions of Jarid2 in transcriptional regulation in *Drosophila*. *Mol. Cell Biol.* 32, 1683–1693.
- Ho, T.T., Warr, M.R., Adelman, E.R., Lansinger, O.M., Flach, J., Verovskaya, E.V., Figueroa, M.E., and Passequé, E. (2017). Autophagy maintains the metabolism and function of young and old stem cells. *Nature* 543, 205–210.
- Hu, Z., Li, H., Jiang, H., Ren, Y., Yu, X., Qiu, J., Stableski, A.B., Zhang, B., Buck, M.J., and Feng, J. (2020). Transient inhibition of mTOR in human pluripotent stem cells enables robust formation of mouse-human chimeric embryos. *Sci. Adv.* 6, eaaz0298.
- Hussein, A.M., Wang, Y., Mathieu, J., Margaretha, L., Song, C., Jones, D.C., Cavanaugh, C., Miklas, J.W., Mahen, E., Showalter, M.R., et al. (2020). Metabolic control over mTOR-dependent diapause-like state. *Dev. Cell* 52, 236–250.e7.
- Hussein, A.M., Balachandar, N., Mathieu, J., and Ruohola-Baker, H. (2022). Molecular regulators of embryonic diapause and cancer diapause-like state. *Cells* 11, 2929.
- Ishibashi, J.R., Keshri, R., Taslim, T.H., Brewer, D.K., Chan, T.C., Lyons, S., McManamen, A.M., Chen, A., Del Castillo, D., and Ruohola-Baker, H. (2021). Chemical genetic screen in *Drosophila* germline uncovers small molecule drugs that sensitize stem cells to insult-induced apoptosis. *Cells* 10, 2771.
- Ishibashi, J.R., Taslim, T.H., and Ruohola-Baker, H. (2020). Germline stem cell aging in the *Drosophila* ovary. *Curr. Opin. Insect Sci.* 37, 57–62.
- Kim, J., and Guan, K.L. (2019). mTOR as a central hub of nutrient signalling and cell growth. *Nat. Cell Biol.* 21, 63–71.
- Klattenhoff, C., Xi, H., Li, C., Lee, S., Xu, J., Khurana, J.S., Zhang, F., Schultz, N., Koppetsch, B.S., Nowosielska, A., et al. (2009). The *Drosophila* HP1 homolog Rhino is required for transposon silencing and piRNA production by dual-strand clusters. *Cell* 138, 1137–1149.
- Landeira, D., Sauer, S., Poot, R., Dvorkina, M., Mazzarella, L., Jørgensen, H.F., Pereira, C.F., Leleu, M., Piccolo, F.M., Spivakov, M., et al. (2010). Jarid2 is a PRC2 component in embryonic stem cells required for multi-lineage differentiation and recruitment of PRC1 and RNA Polymerase II to developmental regulators. *Nat. Cell Biol.* 12, 618–624.
- Laporte, D., Gouleme, L., Jimenez, L., Khemiri, I., and Sagot, I. (2018). Mitochondria reorganization upon proliferation arrest predicts individual yeast cell fate. *Elife* 7, e35685. <https://doi.org/10.7554/eLife.35685>.
- Levy, S., Somasundaram, L., Raj, I.X., Ic-Mex, D., Phal, A., Schmidt, S., Ng, W.I., Mar, D., Decarreau, J., Moss, N., et al. (2022). dCas9 fusion to computer-designed PRC2 inhibitor reveals functional TATA box in distal promoter region. *Cell Rep.* 38, 110457.
- Liang, R., Arif, T., Kalmykova, S., Kasianov, A., Lin, M., Menon, V., Qiu, J., Bernitz, J.M., Moore, K., Lin, F., et al. (2020). Restraining lysosomal activity preserves hematopoietic stem cell quiescence and potency. *Cell Stem Cell* 26, 359–376.e7.
- Lieber, T., Jeedigunta, S.P., Palozzi, J.M., Lehmann, R., and Hurd, T.R. (2019). Mitochondrial fragmentation drives selective removal of deleterious mtDNA in the germline. *Nature* 570, 380–384.
- Ma, X., Han, Y., Song, X., Do, T., Yang, Z., Ni, J., and Xie, T. (2016). DNA damage-induced Lok/CHK2 activation compromises germline stem cell self-renewal and lineage differentiation. *Development* 143, 4312–4323.
- Margueron, R., and Reinberg, D. (2011). The Polycomb complex PRC2 and its mark in life. *Nature* 469, 343–349.
- Martínez-Reyes, I., and Chandel, N.S. (2020). Mitochondrial TCA cycle metabolites control physiology and disease. *Nat. Commun.* 11, 102.
- Mathieu, J., Detraux, D., Kupperts, D., Wang, Y., Cavanaugh, C., Sidhu, S., Levy, S., Robitaille, A.M., Ferreccio, A., Bottorff, T., et al. (2019). Folliculin regulates mTORC1/2 and WNT pathways in early human pluripotency. *Nat. Commun.* 10, 632.
- Matsuda, N., Sato, S., Shiba, K., Okatsu, K., Saisho, K., Gautier, C.A., Sou, Y.S., Saiki, S., Kawajiri, S., Sato, F., et al. (2010). PINK1 stabilized by mitochondrial depolarization recruits Parkin to damaged mitochondria and activates latent Parkin for mitophagy. *J. Cell Biol.* 189, 211–221.
- Mauvezin, C., Ayala, C., Braden, C.R., Kim, J., and Neufeld, T.P. (2014). Assays to monitor autophagy in *Drosophila*. *Methods* 68, 134–139.



- Meng, D., Frank, A.R., and Jewell, J.L. (2018). mTOR signaling in stem and progenitor cells. *Development* 145, dev152595.
- Miklas, J.W., Clark, E., Levy, S., Detraux, D., Leonard, A., Beussman, K., Showalter, M.R., Smith, A.T., Hofsteen, P., Yang, X., et al. (2019). TFPa/HADHA is required for fatty acid beta-oxidation and cardiolipin re-modeling in human cardiomyocytes. *Nat. Commun.* 10, 4671.
- Miklas, J.W., Levy, S., Hofsteen, P., Mex, D.I., Clark, E., Muster, J., Robitaille, A.M., Sivaram, G., Abell, L., Goodson, J.M., et al. (2022). Amino acid primed mTOR activity is essential for heart regeneration. *iScience* 25, 103574.
- Moody, J.D., Levy, S., Mathieu, J., Xing, Y., Kim, W., Dong, C., Tempel, W., Robitaille, A.M., Dang, L.T., Ferreccio, A., et al. (2017). First critical repressive H3K27me3 marks in embryonic stem cells identified using designed protein inhibitor. *Proc. Natl. Acad. Sci. USA* 114, 10125–10130.
- Morita, M., Prudent, J., Basu, K., Goyon, V., Katsumura, S., Hulea, L., Pearl, D., Siddiqui, N., Strack, S., McGuirk, S., et al. (2017). mTOR controls mitochondrial dynamics and cell survival via MTFP1. *Mol. Cell* 67, 922–935.e5.
- Nagy, P., Sándor, G.O., and Juhász, G. (2018). Autophagy maintains stem cells and intestinal homeostasis in *Drosophila*. *Sci. Rep.* 8, 4644.
- Narendra, D., Tanaka, A., Suen, D.F., and Youle, R.J. (2008). Parkin is recruited selectively to impaired mitochondria and promotes their autophagy. *J. Cell Biol.* 183, 795–803.
- Parker, D.J., Iyer, A., Shah, S., Moran, A., Hjelmeland, A.B., Basu, M.K., Liu, R., and Mitra, K. (2015). A new mitochondrial pool of cyclin E, regulated by Drp1, is linked to cell-density-dependent cell proliferation. *J. Cell Sci.* 128, 4171–4182.
- Pauklin, S., and Vallier, L. (2014). The cell-cycle state of stem cells determines cell fate propensity. *Cell* 156, 1338.
- Poole, A.C., Thomas, R.E., Yu, S., Vincow, E.S., and Pallanck, L. (2010). The mitochondrial fusion-promoting factor mitofusin is a substrate of the PINK1/parkin pathway. *PLoS One* 5, e10054.
- Qi, J., Yu, J.Y., Shcherbata, H.R., Mathieu, J., Wang, A.J., Seal, S., Zhou, W., Stadler, B.M., Bourgin, D., Wang, L., et al. (2009). microRNAs regulate human embryonic stem cell division. *Cell Cycle* 8, 3729–3741.
- Rana, A., Oliveira, M.P., Khamoui, A.V., Aparicio, R., Rera, M., Rosziter, H.B., and Walker, D.W. (2017). Promoting Drp1-mediated mitochondrial fission in midlife prolongs healthy lifespan of *Drosophila melanogaster*. *Nat. Commun.* 8, 448.
- Rehman, S.K., Haynes, J., Collignon, E., Brown, K.R., Wang, Y., Nixon, A.M.L., Bruce, J.P., Wintersinger, J.A., Singh Mer, A., Lo, E.B.L., et al. (2021). Colorectal cancer cells enter a diapause-like DTP state to survive chemotherapy. *Cell* 184, 226–242.e21.
- Salemi, S., Yousefi, S., Constantinescu, M.A., Fey, M.F., and Simon, H.U. (2012). Autophagy is required for self-renewal and differentiation of adult human stem cells. *Cell Res.* 22, 432–435.
- Sanjana, N.E., Shalem, O., and Zhang, F. (2014). Improved vectors and genome-wide libraries for CRISPR screening. *Nat. Methods* 11, 783–784.
- Scheckhuber, C.Q., Erjavec, N., Tinazli, A., Hamann, A., Nyström, T., and Osiewicz, H.D. (2007). Reducing mitochondrial fission results in increased life span and fitness of two fungal ageing models. *Nat. Cell Biol.* 9, 99–105.
- Settembre, C., Di Malta, C., Polito, V.A., Garcia Arencibia, M., Vettrini, F., Erdin, S., Erdin, S.U., Huynh, T., Medina, D., Colella, P., et al. (2011). TFEB links autophagy to lysosomal biogenesis. *Science* 332, 1429–1433.
- Shalem, O., Sanjana, N.E., Hartenian, E., Shi, X., Scott, D.A., Mikkelson, T., Heckl, D., Ebert, B.L., Root, D.E., Doench, J.G., and Zhang, F. (2014). Genome-scale CRISPR-Cas9 knockout screening in human cells. *Science* 343, 84–87.
- Somasundaram, L., Levy, S., Hussein, A.M., Ehnes, D.D., Mathieu, J., and Ruohola-Baker, H. (2020). Epigenetic metabolites license stem cell states. *Curr. Top. Dev. Biol.* 138, 209–240.
- Speidel, D. (2010). Transcription-independent p53 apoptosis: an alternative route to death. *Trends Cell Biol.* 20, 14–24.
- Sperber, H., Mathieu, J., Wang, Y., Ferreccio, A., Hesson, J., Xu, Z., Fischer, K.A., Devi, A., Detraux, D., Gu, H., et al. (2015). The metabolome regulates the epigenetic landscape during naive-to-primed human embryonic stem cell transition. *Nat. Cell Biol.* 17, 1523–1535.
- Spurlock, B., Tullet, J., Hartman, J.L., and Mitra, K. (2020). Interplay of mitochondrial fission-fusion with cell cycle regulation: possible impacts on stem cell and organismal aging. *Exp. Gerontol.* 135, 110919.
- Staropoli, J.F., McDermott, C., Martinat, C., Schulman, B., Demireva, E., and Abeliovich, A. (2003). Parkin is a component of an SCF-like ubiquitin ligase complex and protects postmitotic neurons from kainate excitotoxicity. *Neuron* 37, 735–749.
- Sun, N., Youle, R.J., and Finkel, T. (2016). The mitochondrial basis of aging. *Mol. Cell* 61, 654–666.
- Suvorova, I.I., Knyazeva, A.R., Petukhov, A.V., Aksenov, N.D., and Pospelov, V.A. (2019). Resveratrol enhances pluripotency of mouse embryonic stem cells by activating AMPK/Ulk1 pathway. *Cell Death Discov.* 5, 61.
- Tai, H., Wang, Z., Gong, H., Han, X., Zhou, J., Wang, X., Wei, X., Ding, Y., Huang, N., Qin, J., et al. (2017). Autophagy impairment with lysosomal and mitochondrial dysfunction is an important characteristic of oxidative stress-induced senescence. *Autophagy* 13, 99–113.
- Teixeira, F.K., Sanchez, C.G., Hurd, T.R., Seifert, J.R.K., Czech, B., Preall, J.B., Hannon, G.J., and Lehmann, R. (2015). ATP synthase promotes germ cell differentiation independent of oxidative phosphorylation. *Nat. Cell Biol.* 17, 689–696.
- Tie, F., Banerjee, R., Saiakhova, A.R., Howard, B., Monteith, K.E., Scacheri, P.C., Cosgrove, M.S., and Harte, P.J. (2014). Trithorax monomethylates histone H3K4 and interacts directly with CBP to promote H3K27 acetylation and antagonize Polycomb silencing. *Development* 141, 1129–1139.
- van Velthoven, C.T.J., and Rando, T.A. (2019). Stem cell quiescence: dynamism, restraint, and cellular idling. *Cell Stem Cell* 24, 213–225.
- Veeriah, S., Taylor, B.S., Meng, S., Fang, F., Yilmaz, E., Vivanco, I., Janakiraman, M., Schultz, N., Hanrahan, A.J., Pao, W., et al. (2010). Somatic mutations of the Parkinson's disease-associated



- gene PARK2 in glioblastoma and other human malignancies. *Nat. Genet.* **42**, 77–82.
- Villa-Fombuena, G., Lobo-Pecellín, M., Marín-Menguiano, M., Rojas-Ríos, P., and González-Reyes, A. (2021). Live imaging of the *Drosophila* ovarian niche shows spectrosome and centrosome dynamics during asymmetric germline stem cell division. *Development* **148**, dev199716. <https://doi.org/10.1242/dev.199716>.
- Vives-Bauza, C., and Przedborski, S. (2010). PINK1 points Parkin to mitochondria. *Autophagy* **6**, 674–675.
- Wang, L., Shang, Z., Zhou, Y., Hu, X., Chen, Y., Fan, Y., Wei, X., Wu, L., Liang, Q., Zhang, J., and Gao, Z. (2018). Autophagy mediates glucose starvation-induced glioblastoma cell quiescence and chemoresistance through coordinating cell metabolism, cell cycle, and survival. *Cell Death Dis.* **9**, 213.
- Wang, Z.H., Clark, C., and Geisbrecht, E.R. (2016). *Drosophila* clueless is involved in Parkin-dependent mitophagy by promoting VCP-mediated Marf degradation. *Hum. Mol. Genet.* **25**, 1946–1964.
- Wei, Y., Bettedi, L., Ting, C.Y., Kim, K., Zhang, Y., Cai, J., and Lilly, M.A. (2019). The GATOR complex regulates an essential response to meiotic double-stranded breaks in. *Elife* **8**, e42149. <https://doi.org/10.7554/eLife.42149>.
- Wei, Y., Reveal, B., Reich, J., Laursen, W.J., Senger, S., Akbar, T., Iida-Jones, T., Cai, W., Jarnik, M., and Lilly, M.A. (2014). TORC1 regulators Iml1/GATOR1 and GATOR2 control meiotic entry and oocyte development in *Drosophila*. *Proc. Natl. Acad. Sci. USA* **111**, E5670–E5677. <https://doi.org/10.1073/pnas.1419156112>.
- Xing, Y., Su, T.T., and Ruohola-Baker, H. (2015). Tie-mediated signal from apoptotic cells protects stem cells in *Drosophila melanogaster*. *Nat. Commun.* **6**, 7058. <https://doi.org/10.1038/ncomms8058>.
- Yu, J.Y., Reynolds, S.H., Hatfield, S.D., Shcherbata, H.R., Fischer, K.A., Ward, E.J., Long, D., Ding, Y., and Ruohola-Baker, H. (2009). Dicer-1-dependent Dacapo suppression acts downstream of Insulin receptor in regulating cell division of *Drosophila* germline stem cells. *Development* **136**, 1497–1507. <https://doi.org/10.1242/dev.025999>.
- Zhan, Z., Song, L., Zhang, W., Gu, H., Cheng, H., Zhang, Y., Yang, Y., Ji, G., Feng, H., Cheng, T., and Li, Y. (2019). Absence of cyclin-dependent kinase inhibitor p27 or p18 increases efficiency of iPSC generation without induction of iPSC genomic instability. *Cell Death Dis.* **10**, 271. <https://doi.org/10.1038/s41419-019-1502-8>.
- Zhang, T., Zhou, Q., Ogmundsdottir, M.H., Möller, K., Siddaway, R., Larue, L., Hsing, M., Kong, S.W., Goding, C.R., Palsson, A., et al. (2015). Mitf is a master regulator of the v-ATPase, forming a control module for cellular homeostasis with v-ATPase and TORC1. *J. Cell Sci.* **128**, 2938–2950. <https://doi.org/10.1242/jcs.173807>.
- Zhou, W., Choi, M., Margineantu, D., Margaretha, L., Hesson, J., Cavanaugh, C., Blau, C.A., Horwitz, M.S., Hockenbery, D., Ware, C., and Ruohola-Baker, H. (2012). HIF1 α induced switch from bivalent to exclusively glycolytic metabolism during ESC-to-EpiSC/hESC transition. *EMBO J.* **31**, 2103–2116. <https://doi.org/10.1038/emboj.2012.71>.
- Zielke, N., Korzelius, J., van Straaten, M., Bender, K., Schuhknecht, G.F.P., Dutta, D., Xiang, J., and Edgar, B.A. (2014). Fly-FUCCI: a versatile tool for studying cell proliferation in complex tissues. *Cell Rep.* **7**, 588–598. <https://doi.org/10.1016/j.celrep.2014.03.020>.